(12)

NSWC TR 81-97

AD-A143 351

DYNAMIC COMPACTION OF INERT POROUS BEDS

BY H. W. SANDUSKY R. R. BERNECKER A. R. CLAIRMONT, JR.

RESEARCH AND TECHNOLOGY DEPARTMENT

31 OCTOBER 1983

DTIC FILE COPY

Approved for public release, distribution unlimited

NAVAL SURFACE WEAPONS CENTER

Dahlgren, Virginia 22448 • Silver Spring, Maryland 20910

UNCLASSIFIED

SECURITY CLASSIFICATION OF THIS PAGE *(When Data Entered)*

REPORT DOCUMENTATION PAGE	READ INSTRUCTIONS BEFORE COMPLETING FORM
1. REPORT NUMBER NSWC/TR-81-97 ✓	2. GOVT ACCESSION NO. AD-A143351
4. TITLE *(and Subtitle)* DYNAMIC COMPACTION OF INERT POROUS BEDS	5. TYPE OF REPORT & PERIOD COVERED Progress Report June 1979-December 1981
	6. PERFORMING ORG. REPORT NUMBER
7. AUTHOR(s) H. W. Sandusky, R. R. Bernecker, and A. R. Clairmont, Jr.	8. CONTRACT OR GRANT NUMBER(s)
9. PERFORMING ORGANIZATION NAME AND ADDRESS Naval Surface Weapons Center (Code R13) White Oak, Silver Spring, Maryland 20910	10. PROGRAM ELEMENT, PROJECT, TASK AREA & WORK UNIT NUMBERS 61152N; ZR00001; ZR01305; R01AA202
11. CONTROLLING OFFICE NAME AND ADDRESS	12. REPORT DATE 31 October 1983
	13. NUMBER OF PAGES 62
14. MONITORING AGENCY NAME & ADDRESS*(if different from Controlling Office)*	15. SECURITY CLASS. *(of this report)* UNCLASSIFIED
	15a. DECLASSIFICATION/DOWNGRADING SCHEDULE

16. DISTRIBUTION STATEMENT *(of this Report)*

Approved for public release, distribution unlimited.

17. DISTRIBUTION STATEMENT *(of the abstract entered in Block 20, if different from Report)*

18. SUPPLEMENTARY NOTES

19. KEY WORDS *(Continue on reverse side if necessary and identify by block number)*

Dynamic Compaction
Porous Bed Compaction
Deflagration-to-Detonation Transition
DDT
Wave Velocity
Particle Velocity

20. ABSTRACT *(Continue on reverse side if necessary and identify by block number)*

Dynamic compaction is an important process in the deflagration to detonation transition behavior of porous beds of explosives and propellants. The characteristics of gas-driven dynamic compaction fronts have been studied in porous beds of two inert materials, Teflon 7C and melamine. These compaction fronts closely simulate those occurring during the early stages of DDT. In addition, isolation of compaction phenomena is achieved without any complications arising because of ignition and burning of energetic material. Measure-

DD FORM 1 JAN 73 1473 EDITION OF 1 NOV 65 IS OBSOLETE
S/N 0102-LF-014-6601

UNCLASSIFIED
SECURITY CLASSIFICATION OF THIS PAGE *(When Data Entered)*

ments during the dynamic experiments provided wave and particle velocities, density profiles and pressure data.

FOREWORD

The experimental observation at this Center of extensive dynamic compaction in very porous beds of explosives and propellants during deflagration-to-detonation transition (DDT) demonstrated a need to understand the mechanism of dynamic compaction and its role in DDT. This initial study examined the compaction typical of the earliest stage of DDT. The work was accomplished under Task ZR01305, IR-159.

The authors are grateful to Mr. Carl Groves for assembling and instrumenting the experiments and then assisting in conducting them.

Approved by:

Walter F. Proctor, for

JAMES F. PROCTOR, Head
Energetic Materials Division

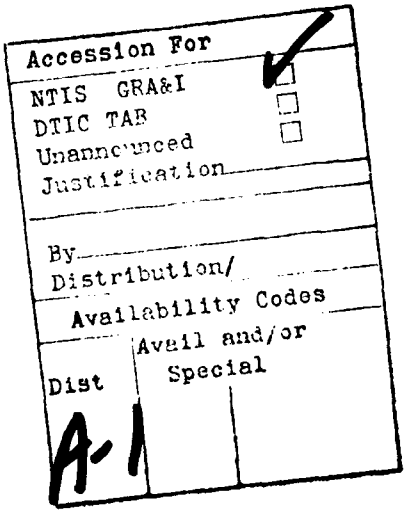

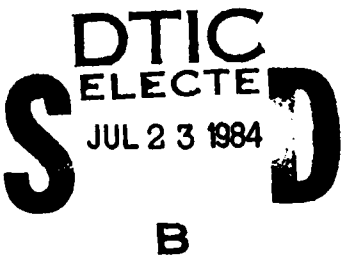

CONTENTS

ILLUSTRATIONS

TABLES

CHAPTER 1

INTRODUCTION

In experimental studies, significant dynamic compaction in very porous beds of explosives and propellants occurs during each stage of the deflagration to detonation transition (DDT) mechanism.[1,2] Even during the several hundred or more microseconds preceding first ignition of an energetic material in the NSWC DDT experiments just referenced, the hot gas ignition source drives a compaction front into the porous bed, reducing the porosity by about 15%. This affects subsequent stages of DDT, such as the spread of ignition through the porous bed by convection of combustion products[3] and the onset of compressive ignition[4] in the final stages of DDT.

This report describes dynamic compaction experiments with compaction rates representative of the early stages of DDT, in particular, the pre-ignition stage described above. Porous beds confined by the NSWC DDT apparatus were compacted by the gas products of the ignitor used in that apparatus. This initial study involved inert granular materials in order to avoid the complications of eventual gas generation from energetic materials, except for possibly some pyrolysis. The inert materials were chosen to represent the variation in mechanical behavior that occurs for plastic bonded explosives and propellants and crystalline explosives. These experiments were part of a research effort[5] that also included: 1) quasi-static compaction measurements of the same materials in order to obtain relationships for intragranular stress versus porous bed density, and 2) the use of these relationships as a compaction law in a numerical model which successfully simulated the dynamic compaction experiments.

CHAPTER 2

EXPERIMENTAL ARRANGEMENT AND PROCEDURE

The apparatus is nearly identical to that described in detail[2] for transparent tube DDT studies. A schematic of an instrumented apparatus is shown in Figure 1a. In most experiments, the porous bed was confined by a clear polycarbonate tube (Lexan, 25.4 mm I.D., 75.6 mm O.D.) clamped between steel plates by four 19 mm bolts. In some experiments, a steel tube with the same inner and outer diameters as a Lexan tube was used to study the effect of increased confinement.

The inert material in the porous beds was either Teflon 7C (du Pont), a polymer with an average particle size (δ) of 30 μM according to the manufacturer, or melamine (Eastman 1540), an organic crystal with $\delta \cong 58$ μm.[6] The theoretical maximum density (TMD) for Teflon 7C was taken to be 2.305 g/cm^3 and that for melamine was taken to be 1.573 g/cm^3. Porous bed density is reported as %TMD or referred to in terms of percent porosity (100 - %TMD). Each porous bed was packed into a tube in either 6.3 mm or 12.6 mm long increments by pouring into the tube the weighed amount of powder for an increment and then consolidating the powder with a ram. In experiments involving flash radiography, a 0.38 mm diameter by 12.5 or 22.9 mm long tungsten wire or a 0.5 to 1.8 mm diameter lead pellet was placed between each increment to serve as an x-ray tracer. The porous beds were about 130 mm long except for one experiment where the bed length was 295 mm.

The ignitor section in the upstream end of the tube is the same as that in a DDT experiment.[2] The ignitor mix (~0.8g of B/KNO_3) is contained in a solid cup that faces the porous bed. Two optical fibers, each terminated by photocells, pass through the end plate and the side of the ignitor cup so that they view the end of the porous bed (see Figure 1 of Reference 2 for details). These optical fibers/photocells were used, just as in DDT experiments, to detect the first appearance of luminous products from the ignitor and then trigger the other recording instrumentation. In some experiments, a slightly undersized thin metal disk (nickel, 25 mm diameter x 0.64 mm thick), that would slide freely in the tube, was placed between the ignitor and the porous bed to inhibit gas flow into the porous bed. In one experiment there was a 4.79 cm^3 cavity between the ignitor and the porous bed to reduce the pressure loading on the bed.

Pressure, bed displacement, and bed density data were available for analysis of most experiments. Pressure was recorded both directly by piezoelectric transducers with their sensing surface in contact with the porous bed and indirectly by strain gages (SG's) bonded to the exterior of the Lexan tubes. The SG's, their measurement circuitry, and their response to steady pressures in a Lexan tube are described in Appendix A. Since measured and

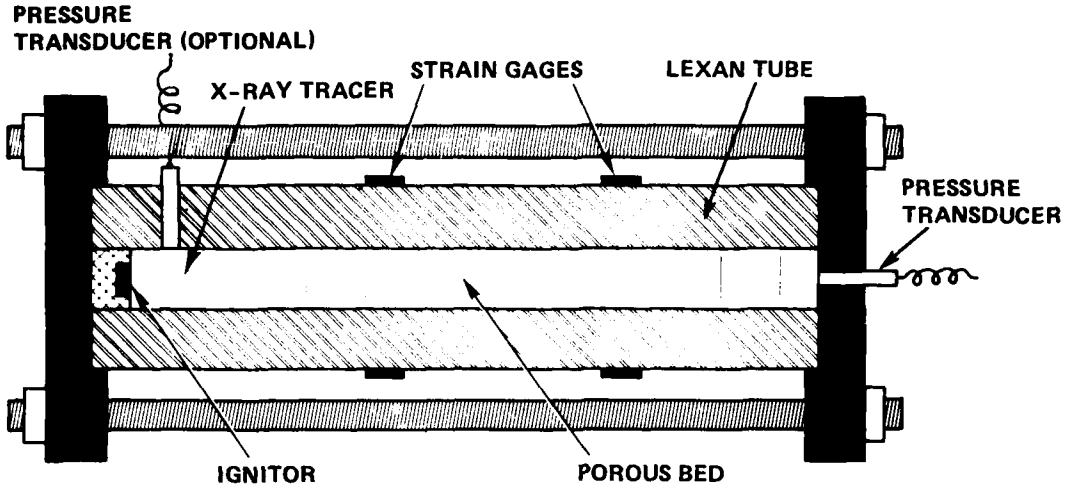

a. SCHEMATIC OF APPARATUS

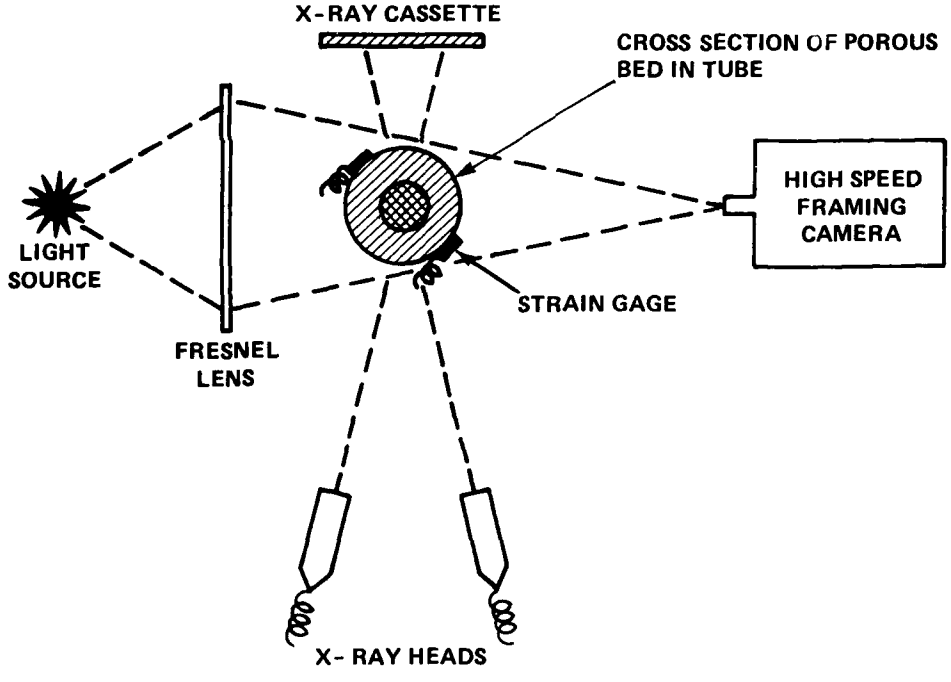

b. ARRANGEMENT OF HIGH SPEED PHOTOGRAPHIC AND FLASH RADIOGRAPHIC INSTRUMENTATION WITH APPARATUS

FIGURE 1. EXPERIMENTAL ARRANGEMENT FOR IGNITOR DRIVEN COMPACTION OF INERT POROUS BEDS

predicted SG output agreed within ±10% for steady pressures in the range of experimental interest (≤15 MPa), all SG output is reported as inner tube wall pressure. In many of the compaction experiments, a piezoelectric transducer (Kistler 607A) was mounted as shown in Figure 1 in order to sense bed pressure at the center of the far boundary. In some experiments, piezoelectric transducers (usually one, a Kistler 607A or PCB 113A23) were mounted in the tube wall near the ignitor.

Lexan tubes are relatively transparent to both light and x-rays. The displacement of the upstream end of the porous bed as a result of compaction was recorded as an expanding zone of luminous ignitor products by either a Beckman Whitley 326 or a Cordin Model 375 framing camera. The film used was Kodak 2484, processed in Kodak D19 developer. The apparatus was backlighted by an electronic flash that was triggered at the same time as the other recording instrumentation in order to synchronize the film data with the other data. As discussed in Reference 2, this method of synchronization is only accurate to within approximately an interframe time (~40 μs) with the B & W Model 326. With the Cordin Model 375, there is a sychronization pulse generated by the camera that, in conjunction with the first appearance of backlighting, accurately indicates (within 2 μs) the time each frame is being exposed.

Compaction of the entire porous bed in Lexan tubes was recorded at two times during each experiment by flash radiographs, and following each experiment another radiograph recorded the final (elastically unloaded) state of compaction. The equipment and setup are described in Reference 2, except no source and film protection were required. The arrangement of flash radiographic and high speed photographic instrumentation with the apparatus is shown in Figure 1b. For steel tubes, radiographs were taken before and after each experiment at the NSWC 2 MV x-ray facility.

CHAPTER 3

EXPERIMENTAL RESULTS

The initial conditions and compaction parameters are summarized in Table 1 for both the melamine and Teflon 7C experiments. The dynamic compaction behavior observed in all experiments was similar to that illustrated by the distance-time (x-t) plot in Figure 2, which is based on Shot S79. For these experiments the size of the particles in the beds and the initial densities of the beds were such that the beds were relatively impermeable to the gaseous products from the ignitor. Therefore, as an ignitor began burning, the pressure at the interface rapidly rose until the yield stress of the bed was exceeded, at which point the bed began to compact. The extension of this compaction process into the porous bed occurred at what will be called the compaction front (CF). The CF is a compressive wave with velocity (U) that increases the initial density, ρ_o^*, to ρ_c^* and imparts a particle velocity, u, to the compacted material. The compacting of the porous bed produced a cavity between itself and the ignitor that was occupied by the luminous ignitor products. This cavity expanded at a rate corresponding to the particle velocity of the compacted material.

For a constant ignitor burning rate, the compaction process procedes at a constant rate, assuming no wall friction. As will be shown later, the ignitor burning is not constant; however, coupling between gas pressure build-up from ignitor burning, gas pressure decline from cavity expansion and the inertia of the already compacted portion of the bed maintain a nearly constant compaction process.

When the CF reaches the rigid far end boundary it reflects as a higher pressure wave which arrests the particle motion and further compacts the porous bed. When this rearward wave reaches the bed cavity interface, a weak compression wave propagates into the gas filled cavity and an expansion wave of the same pressure propagates back into the porous bed. The visible evidence of this is that the zone of luminous ignitor products stops expanding. For most experiments the ignitor burning rate has diminished by this time (about 1 ms) so that subsequent pressure build-up is not sufficient to exceed the pressure that was associated with the rearward wave and thereby further compact the porous bed. The final density, ρ_f^*, is measured in this study after the pressure has been released from each porous bed.

---

*$\rho_x \equiv (TMD)(\%TMD)_x/100$

TABLE 1. SUMMARY OF DATA FROM IGNITOR DRIVEN COMPACTION EXPERIMENTS

		INITIAL CONDITIONS*					COMPACTION PARAMETERS†			
COMPARISON OF EFFECTS	SHOT NO.	POROUS BED MATERIAL	$(\%\ TMD)_o$	IGNITOR BOUNDARY	CONFINING TUBE	L (mm)	u (mm/μs)	U (mm/μs)	$(\%\ TMD)_c$	$(\%\ TMD)_f$
Free volume at the ignitor interface	S92	TEFLON 7C[a]	60.0	CAVITY	LEXAN	133.4	0.007	~0.14		68.2
Different instrumentation	S89-4	TEFLON 7C	60.0	STD	LEXAN	130.2		0.14		
Gas flow into bed	S78	TEFLON 7C	60.0	STD	LEXAN	133.4	0.030	0.14	~80	82.1
Bed length	S79	TEFLON 7C	60.0	DISK	LEXAN	132.8	0.041	0.16	81.9	89.3
	S83	TEFLON 7C	60.0	DISK	LEXAN	295.4	0.041-0.026	0.16	79.7	77.4
Bed confinement	S86	TEFLON 7C	60.0	DISK	STEEL	127.2		0.14		83.5
Bed confinement	S93	MELAMINE[b]	60.0	DISK	STEEL	127.2		0.11		77.1
Gas flow into bed	S77	MELAMINE	60.0	DISK	LEXAN	132.8	0.011	0.11	~69	75.5
Initial density	S69	MELAMINE	60.0	STD	LEXAN	127.0	0.010	0.10	~66	~75
	S7	MELAMINE	70.0	STD	PMMA	155.6	0.013			75.3
	S65	MELAMINE	70.0	STD	LEXAN	138.1	<0.017	~0.27	~75	80.5
	S70	MELAMINE	80.0	STD	LEXAN	127.0	<0.028	~0.42		87.6

*INITIAL CONDITIONS

$(\%TMD)_o$ = Initial relative density
L = Initial bed length
Ignitor boundary:
STD = Face of ignitor in direct contact with porous bed
DISK = Thin metal disk between ignitor and porous bed for inhibiting gas flow into the bed
CAVITY = 4.79 cc cavity between ignitor and porous bed

a. TMD for Teflon 7C = 2.305 g/cc
b. TMD for melamine = 1.573 g/cc

†COMPACTION PARAMETERS

u = Particle velocity behind compaction front
U = Compaction front velocity
$(\%TMD)_c$ = Average axial density behind compaction front
$(\%TMD)_f$ = Average final axial density

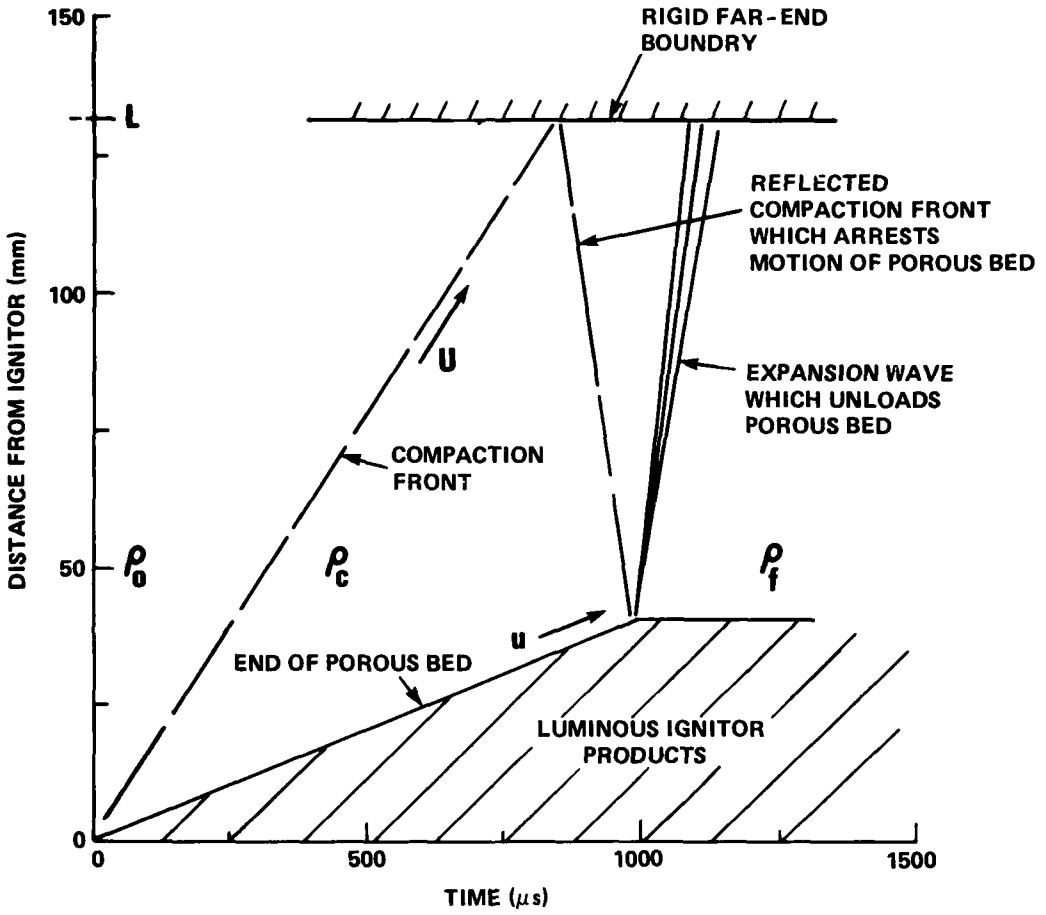

FIGURE 2. IDEALIZED DISTANCE-TIME PLOT FOR IGNITOR DRIVEN COMPACTION (SEE TABLE 1 FOR DEFINITION OF SYMBOLS)

TEFLON 7C EXPERIMENTS

All of the porous beds of Teflon 7C were packed to a density of 1.38 g/cm^3 (60% TMD) which corresponds to 40% porosity (percent of volume not occupied by solid). Other initial conditions were varied to investigate the effects of initial free volume between the ignitor and the porous bed, reduced gas flow into the porous bed, different bed length, and different lateral confinement.

Shot S79

The compaction process in Shot S79, will be discussed first because it most nearly exemplifies the idealized compaction process in Figure 2. This experiment had a thin metal disk over the ignitor which inhibited gas flow into the porous bed of Teflon 7C. In Figure 3a the axial compaction of the porous bed is obtained from the axial displacement of centers of the embedded x-ray tracers. At 498 μs, the tracer closest to the ignitor was displaced by almost 20 mm. Each succeeding tracer was displaced by a lesser amount until tracers beyond 76 mm were not displaced at all. Seventy-six millimeters is defined as the location of the CF at 498 μs; behind this front the initial 60% TMD bed was axially compacted to an average of 81.9% TMD,* except at the ignitor end of the bed which was also radially compacted. Two hundred and fifty-one microseconds later, all the wires displaced before were displaced another 10.1 mm corresponding to a particle velocity of 0.040 mm/μs; the CF had advanced another 41 mm, corresponding to a wave velocity of 0.16 mm/μs. Except at the driven end of the bed, the compaction was still 81.9% TMD.

The compaction process is more easily visualized by plotting %TMD versus x as in Figure 3b for the 498 μs radiography data. The axial compaction profile was computed from the reduced separation between each pair of wires. Because of scatter in the data as well as errors in reading the data, there were variations in density up to 10% for adjacent pairs of wires. Only in Shot S79 was radial compaction observed on the dynamic radiograph; the dashed profile in Figure 3b combines radial and axial compaction. Radial compaction increases the compaction at the driven end of the bed to about 90% TMD, and its contribution extends almost to the CF. It was calculated from measurements of reduced bed diameter assuming uniform cross-sectional density. The calculations were subject to significant error because they are sensitive to small variations in porous bed diameter, which was difficult to measure from the low contrast image on the radiograph.

The propagation of the CF and associated phenomena are illustrated on the distance-time plot in Figure 3c. The luminous ignitor products fill the cavity formed by compaction of the porous bed. The constancy of the compaction process is indicated by the steady expansion of the luminous products which was recorded every 40 μs by the framing camera. The correspondence of the disk location (the ignitor end of porous bed) with the boundary of the luminous zone was verified by the radiographic data. Until 1000 μs, this luminous zone expanded at a rate of 0.041 mm/μs, which corresponds to the 0.040 mm/μs particle

---

*$\rho_C = \rho_O/(1 + s)$, where s = the slope of Δx versus x_i.

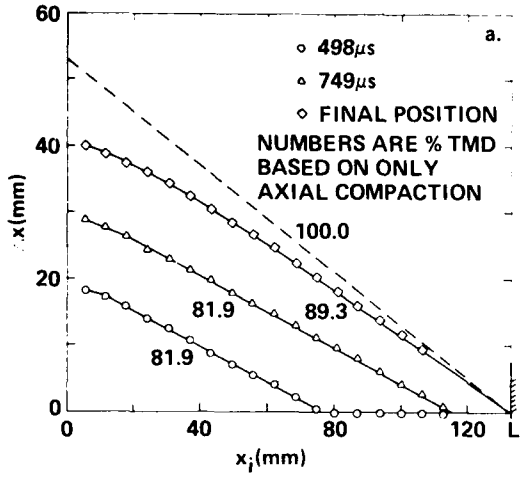

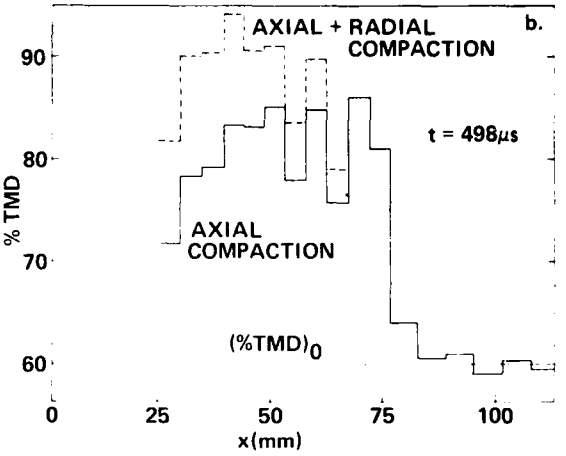

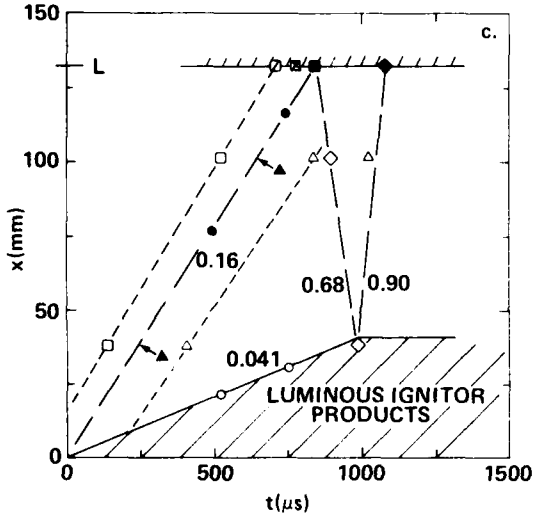

KEY FOR FIGURE 3c.

- ○ ● RADIOGRAPHIC DATA: DISK LOCATION; COMPACTION FRONT LOCATION
- □ △ ◇ STRAIN GAGE DATA: FIRST DETECTION OF STRAIN; ONSET OF STEADY OR DECLINING STRAIN; ONSET OF INCREASING STRAIN
- ▨ ⊠ ■ ◆ PRESSURE TRANSDUCER DATA: FIRST DETECTION OF PRESSURE; ONSET OF RAPID PRESSURIZATION; A PEAK PRESSURE; ONSET OF DECREASING PRESSURE
- ▲ x – t DATA, ARRIVAL OF COMPACTION FRONT AT STRAIN GAGE LOCATION

NUMBERS ARE VELOCITIES (mm/μs)

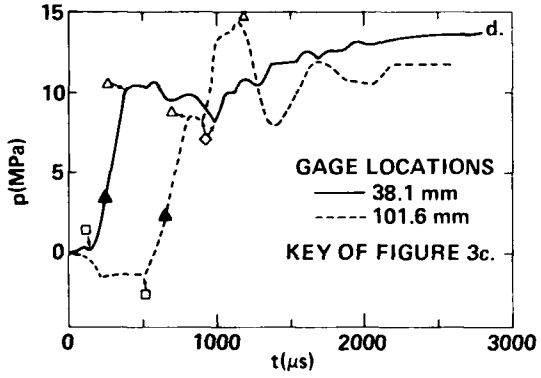

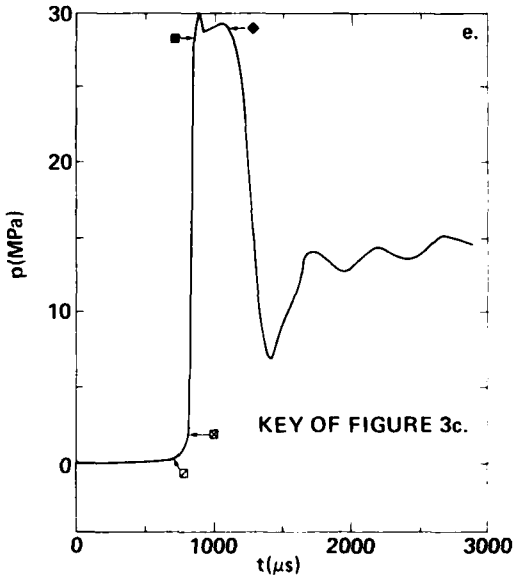

FIGURE 3. DATA FOR IGNITOR/THIN METAL DISK COMPACTION OF 60% TMD TEFLON 7C, SHOT S79
a. AXIAL DISPLACEMENT OF POROUS BED FROM RADIOGRAPHS
b. DENSITY PROFILES AT 498 μs
c. DISTANCE-TIME PLOT
d. STRAIN GAGE TRACES
e. FAR BOUNDARY (132.8 mm) PRESSURE TRANSDUCER TRACE

velocity determined from radiographic data. Since the propagation of the CF and the displacement of the end of the porous bed should originate simultaneously, a straight line representing the path of the CF was drawn through the origin of bed displacement and the two CF locations obtained from radiographic data. Extrapolating the CF path to the far boundary corresponded best with the time that the transducer there recorded its peak pressure. In other experiments, arrival of the CF at the far boundary corresponded to the onset of rapid pressurization there, as expected. Since the 29 μs difference between the two times (compare ⊠ and ■ in Figure 3e) was small in Shot S79, it most likely is experimental error.

Note that preceding the CF path in Figure 3c (by about 120 μs), both SG's and the far boundary transducer first detected strain and pressure. In contrast to the abrupt change in density at the CF seen in the %TMD versus x plot, the 38.1 and 101.6 mm SG's (see Figure 3d) recorded a steadily increasing strain for about 300 μs as the CF passed their locations. Unlike the SG's, the far boundary transducer (see Figure 3e) recorded only a small pressure ahead of the CF relative to the abrupt pressure rise when the CF arrived. This behavior for the SG's and far boundary transducer was also observed in a test of piston driven compaction of Teflon 7C (see Figure A-6 in Appendix A), which avoided complications from gas flow in the porous bed. Explanations for both the premature and slow response of the SG's are postulated in Appendix A.

Following the steady rise in strain from the passage of the CF, the SG's recorded a nearly steady strain corresponding to a pressure of about 10 MPa. Essentially the same pressure, 9.9 MPa, was calculated from jump conditions at the CF ($p = p_o + \rho_o U u$, where $p_o = 0.8$ MPa[9]). The reflection of the CF at the far boundary resulted in a pressure three times as high, 30 MPa, indicating that the compressibility of the porous bed decreased as the density increased. The reflected CF propagated at 0.68 mm/μs, further compacting the porous bed and arresting the 0.041 mm/μs particle velocity. As shown in Figure 3a, the final axial compaction, resulting from the combined effects of the rearward wave and the elastic unloading of the bed when the pressure was eventually released, was 89.3% TMD.

Beyond the far boundary, the reflected CF was first detected by the 101.6 mm SG as an onset of increasing strain (◇ in Figure 3d). When the reflected CF reached the driven end of the bed, 1) the zone of luminous ignitor products stopped expanding, 2) the 38.1 mm SG, which was located near the end of the porous bed in the zone of luminous ignitor products, began recording an increase in strain primarily from residual burning of the ignitor pressurizing a constant volume instead of a previously expanding volume, and 3) an expansion wave began propagating back into the bed to relieve the 30 MPa pressure. The expansion wave was first detected by the 101.6 mm SG as an onset of declining strain (Δ in Figure 3d) and then by the far boundary transducer as a rapid decline in pressure to 7 MPa. The 0.90 mm/μs velocity indicated in Figure 3c for the expansion wave is somewhat less than the longitudinal sound velocity of 1.13 mm/μs measured by Wayne Elban[7] for Teflon 7C at nearly the same compaction, 90.2% TMD; however, the differences in velocity are most likely due to data analysis and interpretation for the compaction experiment. Following the expansion wave, there are additional expansion and elastic compression waves of declining amplitude for about a millisecond. During this time, residual burning of the ignitor continued to pressurize the porous bed to a uniform pressure of about 14 MPa.

Shots S78 and S89-4

Unlike Shot S79, there was not a thin disk over the ignitor end of the 40% porosity beds of Teflon 7C in Shots S78 and S89-4 so that the effect of gas flow into the porous bed could be determined. The instrumentation for Shot S78 was the same as for Shot S79, whereas the only functioning instrumentation for Shot S89-4 was three pressure transducers at different positions along the bed.

When compared to Shot S79, the data for Shot S78 showed that permitting ignitor products to flow into the porous bed reduced the extent of compaction (comparing Figure 4a with 3a) and decreased the density gradient behind the CF (comparing Figure 4b with 3b). The distance-time plot for Shot S78 in Figure 4c is quite similar to the corresponding plot for Shot S79, except in Shot S78 the plateauing of the 38.1 mm SG occurred considerably later than in Shot S79. In Shot S79 both SG's recorded a steady increase in pressure as the CF was passing the SG locations while for Shot S78, as shown in Figure 4d, only the 101.6 mm SG responded in that manner. The 38.1 mm SG trace had a double plateau structure as if two distinct CF's passed the 38.1 mm SG and then coalesced before reaching the 101.6 mm SG. Although the density gradient at the CF is shown in Figure 4b to have increased between the 499 and 756 μs radiograph, there is no evidence of two distinct density steps in the 499 μs radiograph. This same type of SG trace (double plateau structure) occurred in Shot S77 (see Figure 11c), which involved 60% TMD melamine with a disk at the ignitor interface; so restricting gas flow into the porous bed does not necessarily exclude this type of SG trace. The loss of pressure transducer data in Figure 4e above 15 MPa resulted from the transducer output exceeding the voltage range chosen for the oscilloscope.

For Shot S89 there were mounted into the Lexan tube two recessed pressure transducers: one at the ignitor interface and another at 37.4 mm. From the inner tube wall, a 1.4 mm diameter by 4 mm long channel opened into a cavity that was the diameter of the transducer, about 6.3 mm, and less than 1 mm long. The purpose of this arrangement was to measure gas pressure without influence from the solid stress on the inner tube wall. The small diameter of the channel was chosen assuming that a small unsupported area on the porous bed would prevent bed break-up and the plugging of the channel; however, a small channel inhibits rapid response of the transducer to gas pressure.

Shot S89 was instrumented the same as Shot S78 except for the additional recess mounted transducers, but no data were obtained because of mistakes during setup of the experiment. Because the Lexan tube was intact following the experiment, it was prepared for a repeat experiment. The inner tube wall was not optically clear enough at the ignitor for good photographic coverage, so the tube was reloaded for an experiment, Shot S89-4, to record just the responses of the pressure transducers and the strain gages. However, the strain gages responded so erratically that their output could not be analyzed.

The pressure transducer responses for Shot S89-4 are shown in Figure 5. At the ignitor the pressure obtained a relatively steady level of 7 $\pm$ 1 MPa in less than 100 μs. A CF velocity of 0.14 mm/μs, which agrees with that from Shot S78, is calculated based on the first response (-10 μs) of the transducer at the ignitor interface and the onset of rapid pressurization (950 μs) at the far boundary transducer. A velocity of 0.10 mm/μs is calculated based on the first responses of the transducers at 0.0 and 37.4 mm. This is an indication of the

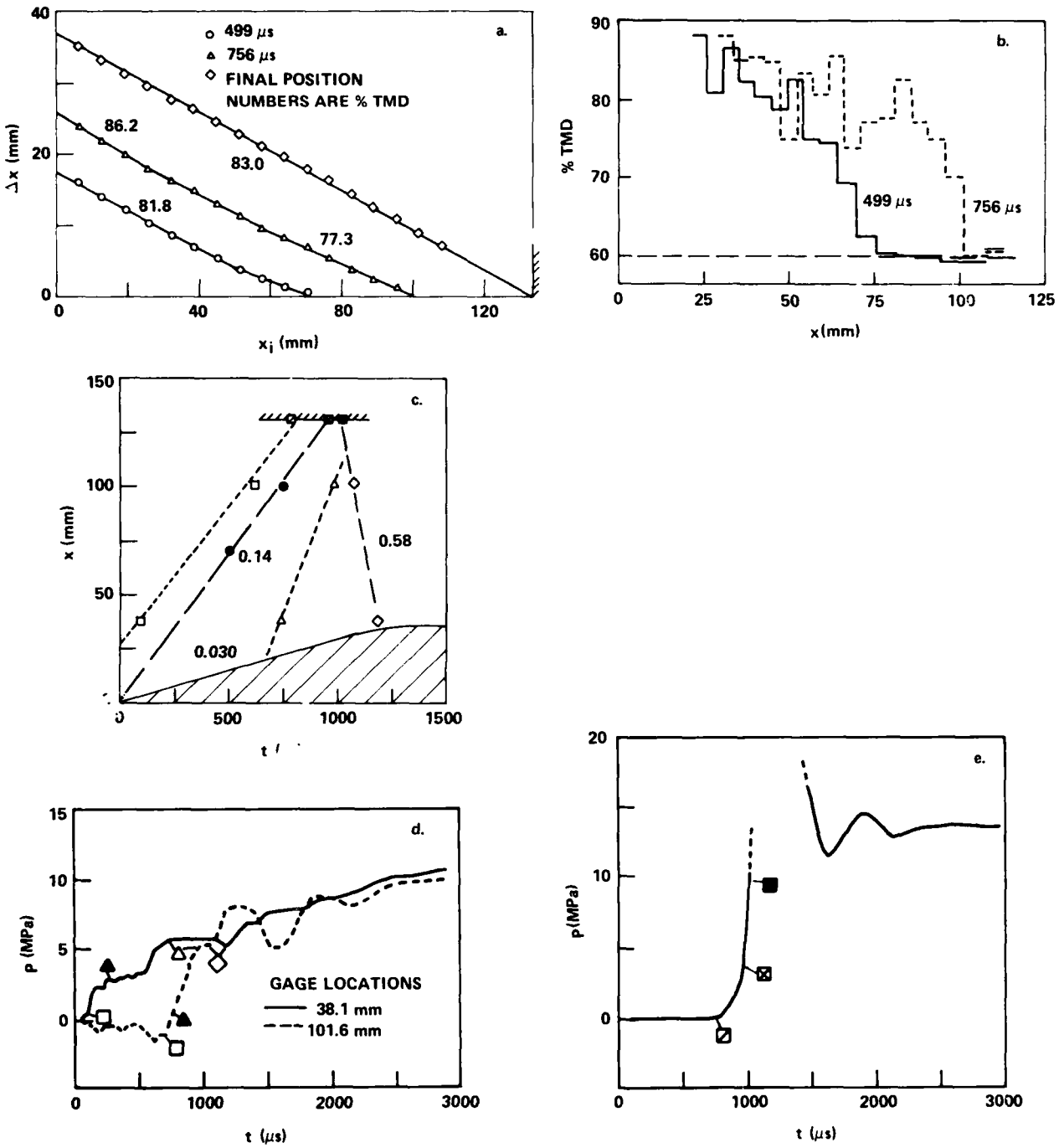

FIGURE 4. DATA FOR IGNITOR COMPACTION OF 60% TMD TEFLON 7C, SHOT S78
(REFER TO FIGURE 3 FOR THE KEY)
a. AXIAL DISPLACEMENT OF POROUS BED FROM RADIOGRAPHS
b. DENSITY PROFILES FROM RADIOGRAPHIC DATA
c. DISTANCE-TIME PLOT
d. STRAIN GAGE TRACES
e. FAR BOUNDARY (133.4 mm) PRESSURE TRANSDUCER TRACE

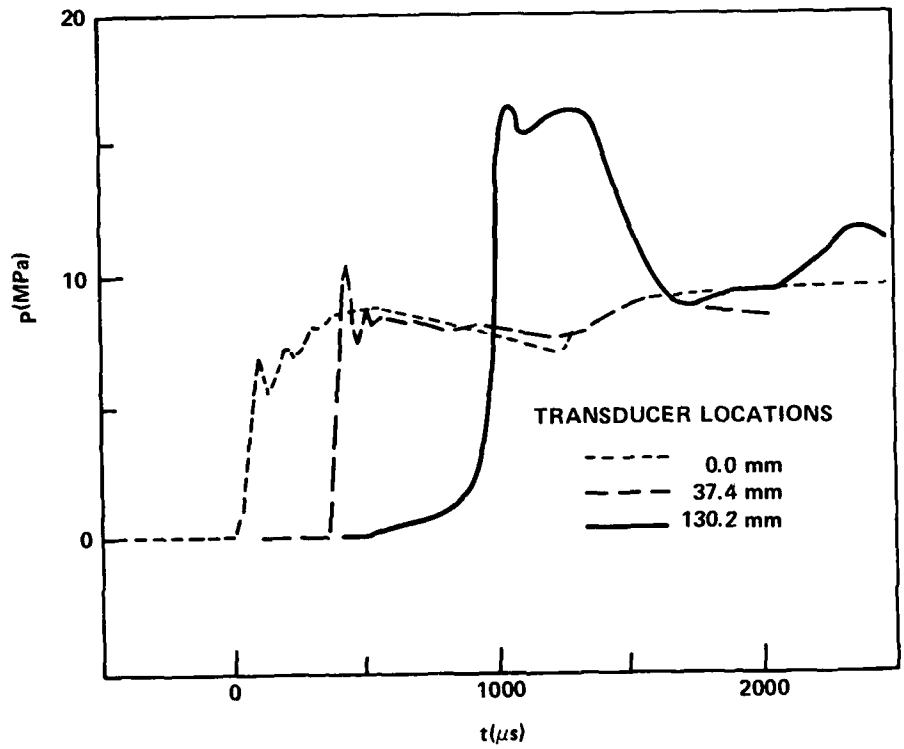

FIGURE 5. PRESSURE TRANSDUCER TRACES FROM IGNITOR COMPACTION OF 60% TMD TEFLON 7C, SHOT S89-4

rate of gas flow since the recessed transducers should respond only to gas pressure. That gas probably flowed almost exclusively along the inner tube wall. If the gas filtered through the porous bed, the rapid rise in pressure at 37.4 mm to the same pressure at the ignitor interface would not be expected. Gas flow along the inner tube wall occurred at some point in all the plastic tube experiments. After each experiment a large portion of the inner tube wall over the entire length of the bed would be blackened by ignitor products, and as mentioned before, in Shot S79 a gap at the inner tube wall was radiographed during the propagation of the CF.

Shot S92

In Shot S92 there was a 4.8 cm^3 cavity, 16.5 mm in diameter by 22.4 mm long, between the ignitor and the 60% TMD porous bed of Teflon 7C. The cavity allowed a more gentle pressure build-up from the ignitor, a so called "soft ignitor". The soft ignitor is of interest to DDT studies for investigating the effect of ignitor variations - in particular, rate of pressurization - on the build-up to DDT.

Instrumentation for Shot S92 included high speed photography, flash radiograms at 501 and 752 μs, and a pressure transducer at the far boundary. A pressure transducer was also located at the far end of the cavity for comparing the pressure build-up with that at the ignitor interface in Shot S89-4, but the transducer was defective and no data could be recorded.

The framing camera film showed the far end of the porous bed to begin moving at about 500 μs at a rate of ~0.007 mm/μs, which was considerably slower than in the other experiments. The radiograph at 501 μs showed slight movement (0.4 mm) of the end of the porous bed with a mass of ignitor mix adjacent to it. The radiograph at 752 μs showed 1.0 mm movement of the end of the porous bed with the mass of ignitor mix still adjacent to it but reduced in size. Without the porous bed initially adjacent to the ignitor mix, as in other experiments, there is no axial restraint on the ignitor mix; initial burning in the closed end of the cup near the bridgewire can propel the ignitor mix from the cup. The removal of ignitor mix from the cup probably reduces the spread of ignition through the ignitor mix, thereby altering the ignitor mass generation. So pressure build-up on the end of the porous bed is affected by both the volume of the cavity and changes in the burning of the ignitor mix.

Unlike Shot S78, the pressure at the far boundary of the porous bed in Shot S92, see Figure 6, increased very gradually for about 600 μs before the more rapid build-up associated with the CF. In Shot S89-4, see Figure 5, there was also an initial gradual build-up in pressure. For both Shots S92 and S89-4, the initial pressure build-up was small enough in magnitude to be elastic loading of the porous bed according to quasi-static data.[5]

Relative to the first detection of luminosity at the ignitor interface, the arrival of the CF at the far boundary was about 600 μs later than that in Shots S78 and S89-4. This, in conjunction with the later start of the CF (~500 μs), indicates that the CF velocity was nearly the same as in Shots S78 and S89-4, as expected because CF velocity is a weak function of pressure (see Chapter 4).

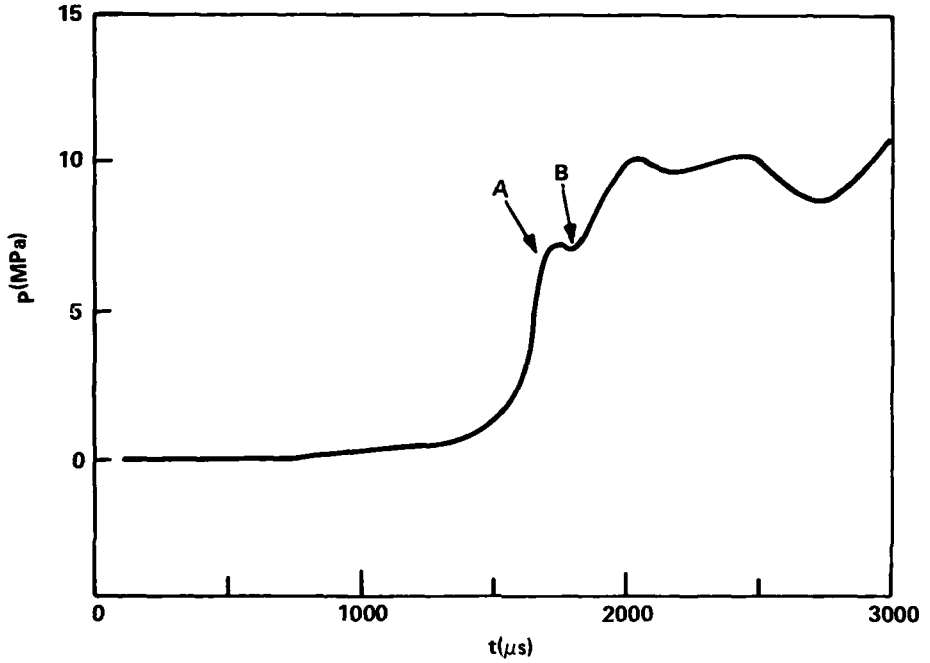

FIGURE 6. FAR BOUNDARY (133.4mm) PRESSURE TRANSDUCER TRACE FROM IGNITOR/FREE VOLUME COMPACTION OF 60% TMD TEFLON 7C, SHOT S92

The pressure transducer trace shown in Figure 6 is unique compared to the other far boundary transducer traces. Following the arrival of the CF, the pressure peaks at time "A", plateaus for ~100 μs, and then at time "B" starts rising again to a relatively steady pressure of about 10 MPa. One explanation for the second pressure rise, beginning at time "B", is that gas flowed along a gap between the porous bed and the inner tube wall. When comparing the radiograph preceding the experiment, see Figure 7a, with that following the experiment, see Figure 7b, significant radial compaction, more than in any other experiment, is evident in the radiograph following the experiment. This radial compaction occurred after the radiograph at 752 μs and so it probably did not precede the CF. Had the radial compaction followed the CF by about 100 μs, the pressure trace in Figure 6 would result. Another explanation for the second pressure rise is that it represents a second CF that was ~100 μs behind the first because of the altered ignitor mass generation rate.

Shot S83

The longer bed length of Shot S83 (more than twice those of other Teflon 7C experiments) allowed for more temporal resolution of the various forward and reflected waves. Other than for the increased bed length of Shot S83, the experiment was like Shot S79, including the disk separating the ignitor and Teflon 7C, except for some additional instrumentation - a pressure transducer in the Lexan tube wall at 25.4 mm and a SG at 190.5 mm.

As expected, the data in Figure 8 show compaction phenomena in the first half of the porous bed nearly identical with that observed in Shot S79. However, the ignitor action did not persist long enough to maintain the same compaction for the second half of the porous bed. The trace for the 25.4 mm transducer in Figure 8d shows that once a peak pressure was reached at about 250 μs, the pressure continuously declined until about 2500 μs when the rearward CF had reached the ignitor end of the porous bed. The lower pressures resulted in the particle velocity declining to 0.026 mm/μs from the initial 0.041 mm/μs, as shown in Figure 8b; apparently the CF velocity remained the same. Also, the peak pressure shown for the far boundary in Figure 8d is only about half that shown in Figure 3e for the far boundary in Shot S79, and the final compaction of 77.4% TMD shown in Figure 8a is 11.9% less than the final compaction for Shot S79.

Unlike previous experiments, the final compaction for Shot S83 is less than the compaction at earlier times in the first half of the bed. Apparently the 13.5 MPa strength of the rearward wave seen by the 295.4 mm transducer declined so rapidly that the peak 9.1 MPa pressure on the driven end of the bed seen by the 25.4 mm transducer was never exceeded except just at the far end of the bed. Therefore, the driven end of the bed was not further compacted by the rearward wave and following the experiment, when the pressure was released and the bed relaxed, elastic unloading of the bed reduced the density by 2%.

The response of the first two SG's to the CF, as shown in Figure 8c were quite similar to the responses at the same gage locations in Shot S79 (see Figure 3d). However, the gage responses to the rearward compaction wave differed in the two shots due to the longer bed length in Shot S83. What is surprising in Shot S83 was the response of the third SG at 190.5 mm; the first response of this gage occurred much sooner than expected, corresponding to a phenomenon with a velocity

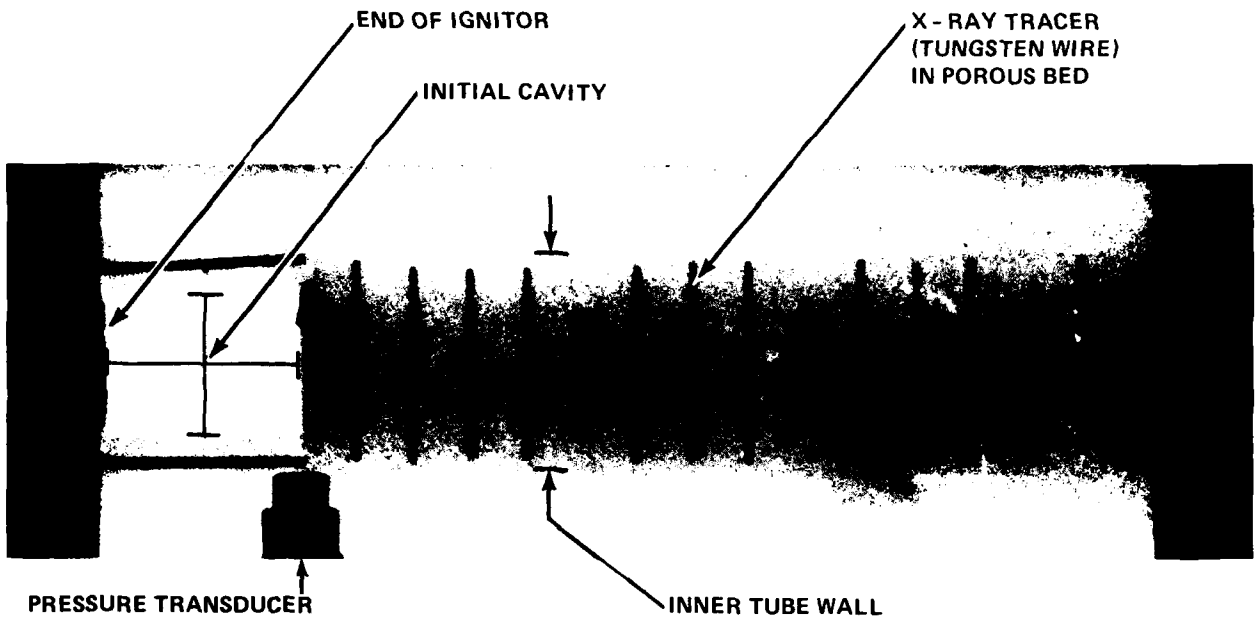

a. BEFORE THE EXPERIMENT

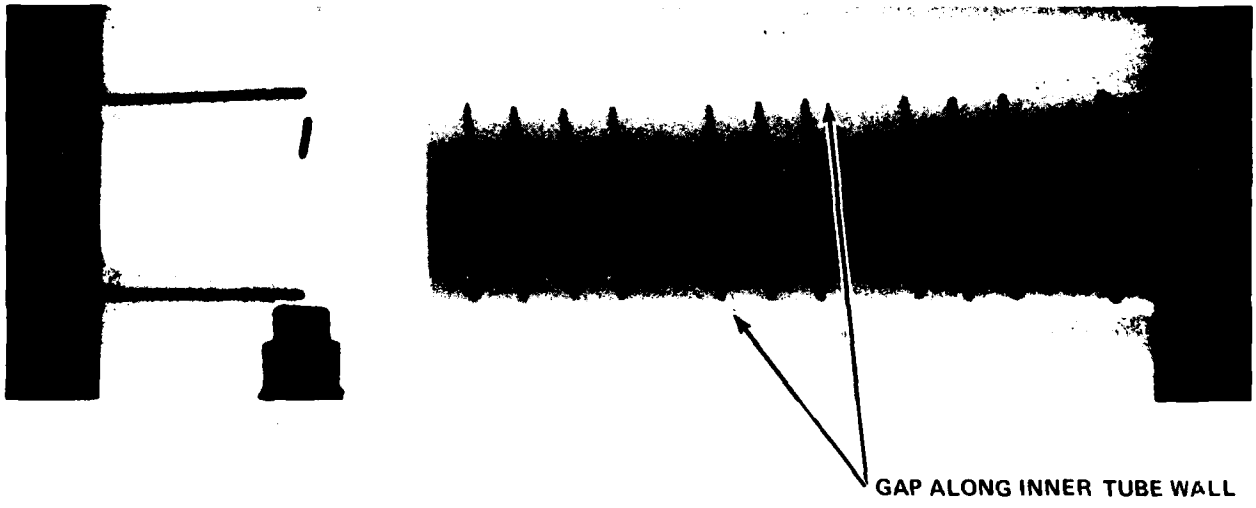

b. AFTER THE EXPERIMENT

FIGURE 7. FLASH X-RAYS OF SHOT S92 BEFORE (a.) AND AFTER (b.) THE EXPERIMENT

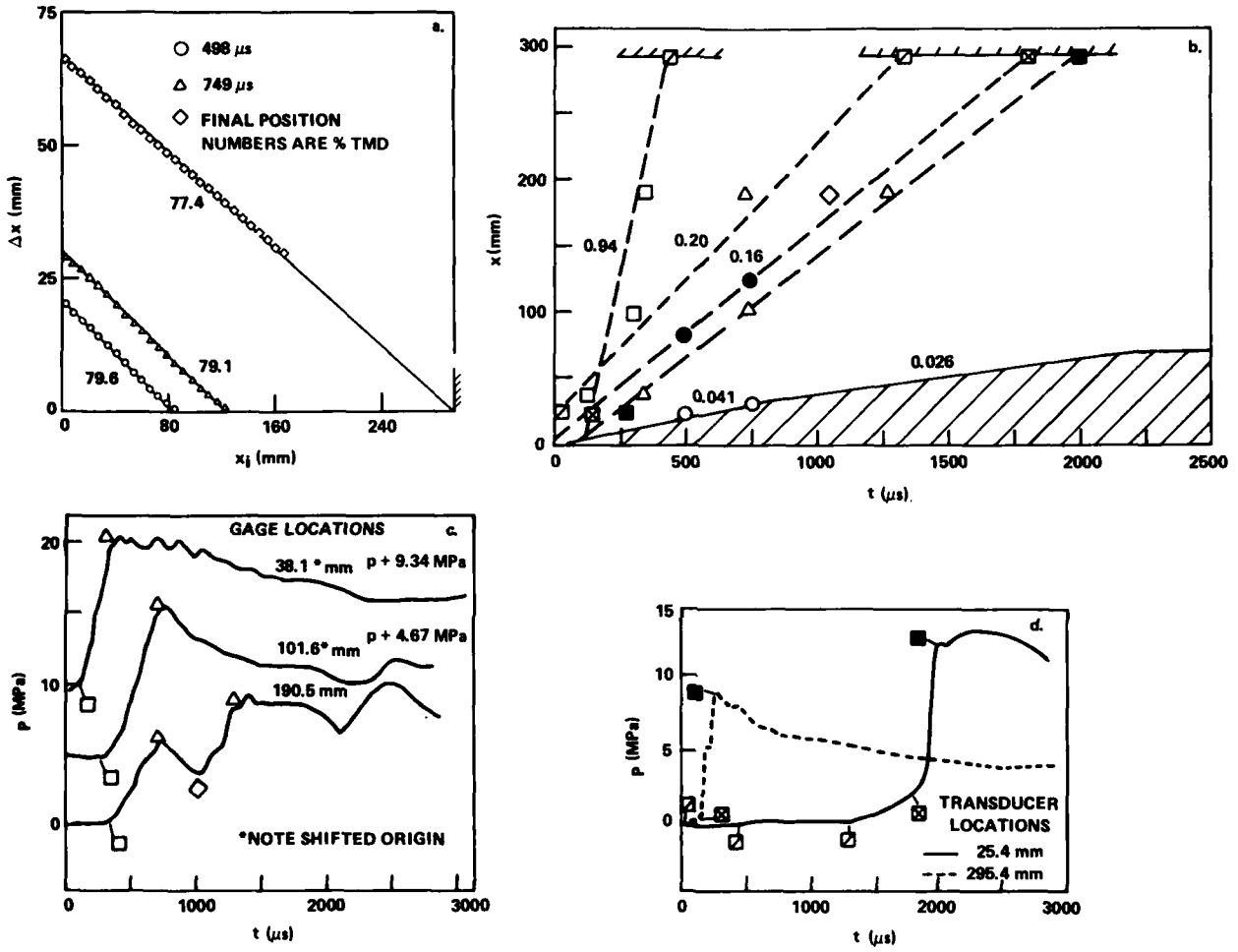

FIGURE 8. DATA FOR IGNITOR/THIN METAL DISK COMPACTION OF 60% TMD TEFLON 7C, SHOT S83 (REFER TO FIGURE 3 FOR THE KEY)
a. AXIAL DISPLACEMENT OF POROUS BED FROM RADIOGRAPHS
b. DISTANCE-TIME PLOT
c. STRAIN GAGE TRACES
d. PRESSURE TRANSDUCER TRACES

of 0.94 mm/μs if a straight line is drawn that approximately connects the first reponse of all gages and an almost indistinguishable first response by the far boundary transducer. In addition to the high velocity of this phenomenon, there was at 190.5 mm a significant build-up of strain at a rate somewhat less than the strain rate at the previous gage. However, before the CF reached the SG location, the strain peaked, declined at a rate similar to its rise, but then increased again as the CF approached the SG location. At least during the initial rise in strain there was hardly any pressure measured by the far boundary transducer, indicating that the phenomenon was not a solid stress wave in the Teflon 7C. The SG response testing discussed in the Appendix, especially the results referred to in Figure A-4b, suggest that a response similar to that of the 190.5 mm SG for the first millisecond will result from gas flow along the inner tube wall. It can be postulated that the decline in strain at the 190.5 mm SG location beginning at ~700 μs resulted from declining gas flow along the inner tube wall as the pressure near the ignitor declined. This gas flow reached the far boundary transducer beginning at ~1350 μs.

Shot S86

It would simplify dynamic compaction experimentation and modeling if wall effects were insignificant, especially, as will be shown, for melamine. The wall effects include friction between the porous bed and the inner tube wall, preferential channeling of gas flow along the inner tube wall, and heat loss to the inner tube wall in the zone between the ignitor and the driven end of the porous bed. Anytime there is preferential gas flow along the inner tube wall, as is often the case in DDT experiments,[2] the wall has separated from the porous bed either because of radial compaction or tube expansion or both; in any case, wall friction is eliminated. This compaction study primarily used Lexan tubes in order to observe the compaction processes by high speed photography and flash radiography, and to better simulate compaction in DDT studies which use the same tubes. These tubes maintain low confinement of a porous bed relative to steel tubes, which because of their high strength, were selected to investigate compaction without inner wall gas flow from tube expansion. Even the slightest tube expansion would allow gas to seep along the inner tube wall and then radially compact the porous bed thus allowing an annulus for gas flow to continue the process to the far boundary. Since the steel tube compaction experiments (Shots S86 and S93), an experiment involving a tight fitting plug in a Lexan tube (see Figure A-4 and the associated discussion in the Appendix) indicated that tube expansion, for the pressures of interest in this study, allowed little gas flow along the tube wall.

In Shot S86, with the exception of the steel tube confinement, the 60% TMD Teflon porous bed was like that in Shot S79; there was a free sliding disk on the driven end of the bed, x-ray tracers in the porous bed, and a pressure transducer at the far boundary. Another pressure transducer was mounted in the tube wall at 25.4 mm, like Shot S83.

The steel tube for Shot S86 was radiographed at the NSWC 2 MV x-ray facility before and after the experiment. From those radiographs the final extent of compaction was measured as 79.7% TMD for the first third of the porous bed and 85.6% TMD for the remainder of the bed; average compaction was 83.5% TMD. The lower axial density for the first third of the bed would suggest radial

compaction as in Shot S79, but no radial compaction was visible on the radiographs. However, the pressure transducer outputs might indicate gas flow along the inner tube wall in an annulus caused by radial compaction, before the CF reached the far boundary. Comparing the 25.4 mm transducer trace in Figure 9 with that from Shot S83 in Figure 8d shows that both transducers began responding similarily to the initial pressure rise, but that the Shot S83 transducer recorded a peak pressure of ~9 MPa followed by a decline in pressure whereas in Shot S86 the transducer recorded a 6.7 MPa peak pressure followed by an eventual increase in pressure. The lower peak pressure in Shot S86 is possibly from the onset of gas flow along the inner tube wall; that gas flow appeared as the gradual rise in pressure preceding the CF at the far boundary. Another possibility for the different pressure traces is variation in ignitor burning rates.

Even though the bed in Shot S86 was 5.6 mm shorter than in Shot S79, the far boundary pressure for Shot S79 (see Figure 3e) peaked about 14 MPa higher than in Shot S86 and the average axial density was about 6.5% higher in Shot S79. Also, the 0.16 mm/μs CF velocity in Shot S79 was higher than the 0.14 mm/μs velocity, based on transducer responses, in Shot S86. It is unlikely that wall friction had much influence since the coefficient of static friction for Teflon[8] (sliding friction was not listed for Teflon in Reference 8) is not only low, 0.04, but the same for Teflon in contact with itself or steel. Certainly the steel tube would absorb more heat from the ignitor products than a plastic tube and thereby reduce the gas pressure; this effect also would be more pronounced if gas flowed along the inner tube wall rather than remain in the cavity between the ignitor and the disk. However, since the pressure continued to increase slowly after 1500 μs from residual burning of the ignitor, it seems unlikely that heat loss was significant. A remaining possibility for reduced compaction in Shot S86 relative to Shot S79 is variation in ignitor burning rates, which is considered further in the following discussion for Shot S93.

MELAMINE EXPERIMENTS

The events observed during dynamic compaction of melamine were similar yet also different than in Teflon 7C because, as discussed in Reference 5, melamine is less compressible and has higher wall friction. Unlike the Teflon 7C experiments, the melamine beds were packed at three differing initial densities to explore this effect. Although the melamine experiments are discussed after those for Teflon 7C, the melamine experiments were performed first, except for Shot S93; and because the instrumentation was developed during the initial experiments, there were less data than in the Teflon 7C shots. For convenience, the melamine data in Table 1 are shown in Table 2.

Shot S93

The melamine was packed at 60% TMD with a disk separating the ignitor and the bed in the same tube as in Shot S86, except that an additional pressure transducer was mounted in the tube with its sensing surface at the inner tube wall, adjacent to the ignitor interface. The pressure at the ignitor, see Figure 10, increased much more slowly than the pressure at the ignitor shown in Figure 5 for Shot S89-4. Because melamine is less compressible than Teflon 7C, the final

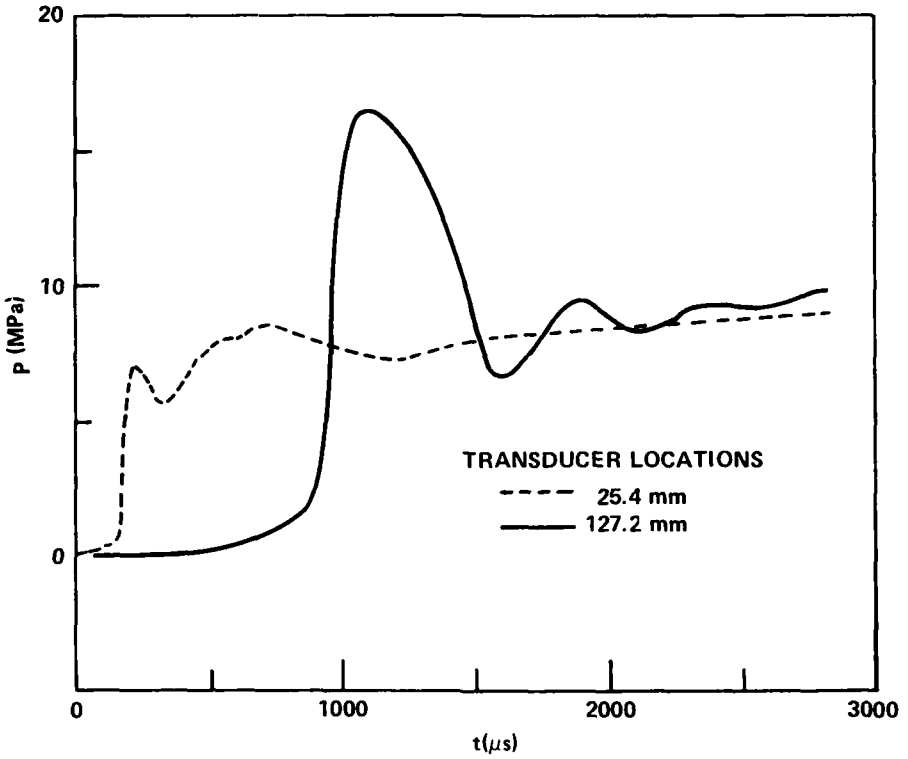

FIGURE 9. PRESSURE TRANSDUCER TRACES FROM IGNITOR/THIN METAL DISK COMPACTION OF 60% TMD TEFLON 7C IN A STEEL TUBE, SHOT S86

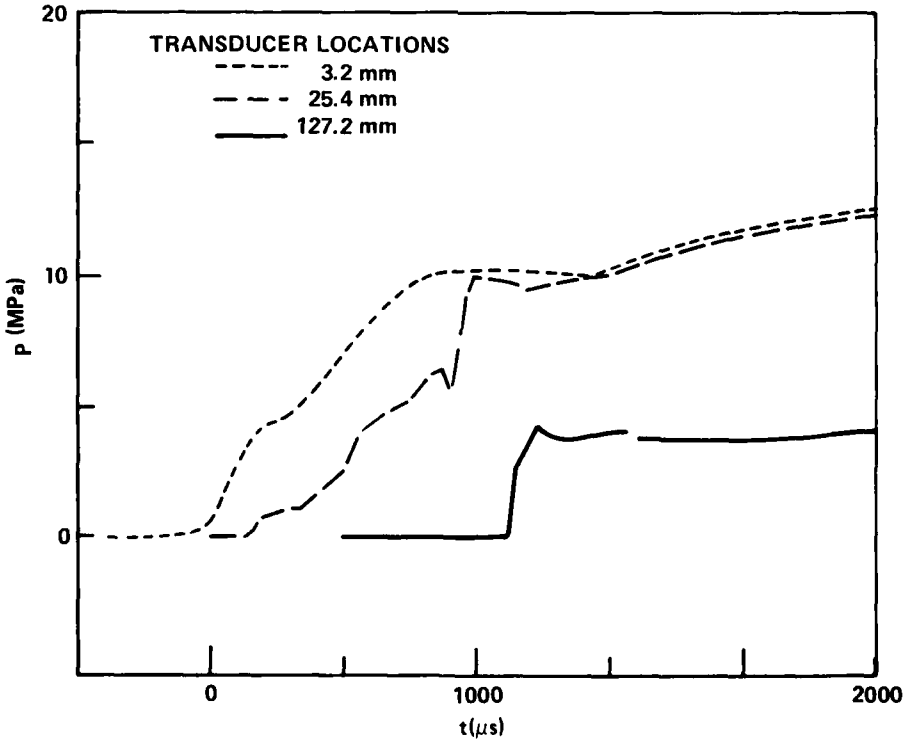

FIGURE 10. PRESSURE TRANSDUCER TRACES FROM IGNITOR/THIN METAL DISK COMPACTION OF 60% TMD MELAMINE IN A STEEL TUBE, SHOT S93

TABLE 2. MELAMINE DATA FROM TABLE 1*

	INITIAL CONDITIONS				COMPACTION PARAMETERS			
SHOT NO.	$(\% \text{ TMD})_o$	IGNITOR BOUNDARY	CONFINING TUBE	L (mm)	u (mm/μs)	U (mm/μs)	$(\% \text{ TMD})_c$	$(\% \text{ TMD})_f$
S93	60.0	DISK	STEEL	127.2		0.11		77.1
S77	60.0	DISK	LEXAN	132.8	0.011	0.11	~69	75.5
S69	60.0	STD	LEXAN	127.0	0.010	0.10	~66	~75
S7	70.0	STD	PMMA	155.6	0.013			75.3
S65	70.0	STD	LEXAN	138.1	<0.017	~0.27	~75	80.5
S70	80.0	STD	LEXAN	127.0	<0.028	~0.42		87.6

*See Table 1 for definition of parameters.

pressure at the ignitor was higher in Shot S93; likewise, the rate of pressurization should have been higher. Although the ignitors in both experiments were from the same batch, it was proposed that variations in burning rate caused the discrepancy in rate of pressurization. So separate tests were conducted to check the consistency of ignitor burning, but test results were ambiguous because of the difficulty in designing an appropriate test.

The transducer responses in Figure 10 indicate that the CF velocity was 0.11 mm/μs based on the first response of each transducer. The sharp rise in pressure at the far boundary to a lower pressure than at the ignitor indicates a distinct density jump at the CF but that wall friction had considerably attenuated the CF pressure. There was no gas flow to the far boundary since there was no pressure increase after the reflection of the CF (note the pressure gradient between the two ends of the compacted column).

As in Shot S86, the porous bed was radiographed before and after the experiment. The final compaction for the first third of the bed was 73.8% TMD, and for the remainder of the bed it was 77.5% TMD; an average compaction for the entire bed was 77.1% TMD. This average density, the CF velocity, and the far boundary transducer trace are quite similar to Shot S77 data, which had the same porous bed configuration in a Lexan tube.

Shot S77

Sixty percent TMD melamine, with a disk at the ignitor interface, was packed into a Lexan tube. The dynamic radiography data in Figure 11a show more compaction at the driven end of the bed than just behind the CF. Based on this data, the particle velocity steadily increases from 0.011 mm/μs (the value in Table 2) at the CF to 0.019 mm/μs at the driven end of the bed, which agrees well with the 0.020 mm/μs rate of expansion for the luminous ignitor products shown in Figure 11b. The decline in density and particle velocity from the driven end of the compacted zone to the CF was due to the pressure attenuation indicated by SG data.

The SG data in Figure 11c and the far boundary transducer data in Figure 11d contain features that contrast with the Teflon 7C data. For melamine the SG data did not show any significant increase in strain preceding the CF (see Figure 11b), there was less recorded strain when the CF passed the 38.1 mm SG location than when it passed the 101.6 mm SG location, and the CF reflected at the far boundary with a pressure less than the ignitor product pressure. Even after 3000 μs, the pressure had not equilibrated throughout the porous bed indicating that there was little gas flow along the inner tube wall. As shown in the Appendix, significant gas flow along the inner wall requires some radial compaction to form an annulus at the wall. Thus the porous bed maintained contact with the inner tube wall and was restrained by friction, which according to quasi-static data[5] is an order of magnitude higher than for Teflon 7C.

Shot S69

As shown in Table 2, removing the disk from the driven end of the 60% TMD melamine bed for Shot S69 resulted in 3% TMD less compaction just behind the CF. As in Shot S77, the density determined from the dynamic radiographs (see Figure

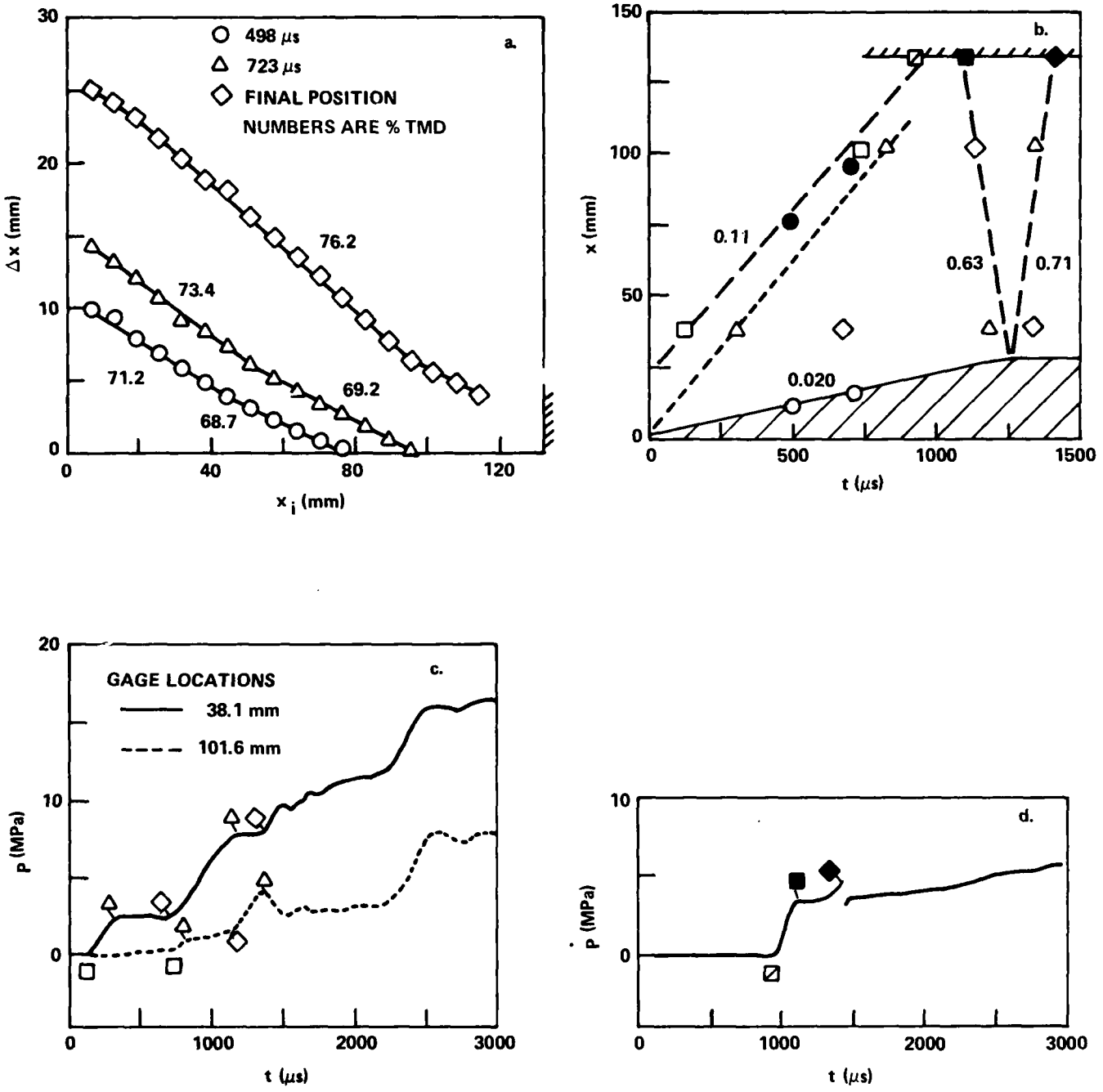

FIGURE 11. DATA FOR IGNITOR/THIN METAL DISK COMPACTION OF 60% TMD MELAMINE, SHOT S77 (REFER TO FIGURE 3 FOR THE KEY)
a. AXIAL DISPLACEMENT OF POROUS BED FROM RADIOGRAPHS
b. DISTANCE-TIME PLOT
c. STRAIN GAGE TRACES
d. FAR BOUNDARY (132.8 mm) PRESSURE TRANSDUCER TRACE

12a) for the compacted zone was higher near the driven end, and the particle velocities based on this data increased from 0.010 mm/μs (the value in Table 2) at the CF to 0.012 mm/μs at the driven end, which corresponds to the 0.013 mm/μs rate of expansion of the luminous ignitor products (see Figure 12b).

Note that the distance-time plots for both Shot S77 (see Figure 11b) and Shot S69 show the CF originating about 250 μs ahead of the luminous ignitor products; however, the CF cannot originate before particle motion. Compaction phenomena, such as a decelerating CF (note locations of CF according to radiographs in Figure 11b) or an initially lower particle velocity, may be responsible. Also possible is the analysis of data; for example, the initial exposure on the camera film from the ignitor products is weak and makes data reduction difficult.

Both the SG and transducer traces in Figures 12c & d for Shot S69 indicate pressures which are only half of those pressures measured in Shot S77. Since the final extent of compaction was essentially the same as in Shot S77, it appears in Shot S69 that the dissipation of ignitor product pressure, the driving force for compaction, by gas flow into the porous bed was smaller than indicated by the difference between recorded pressures in Shot S69 and S70. It is postulated that the disk in Shot S77 promoted a small flow of gas along the inner tube wall, thus increasing measured pressures. An indication of this may be seen in the far boundary transducer traces. In Figure 12d (Shot S69) the increased pressure following reflection of the CF was reduced by an expansion wave as expected, whereas in Figure 11d (Shot S77) the pressure following reflection of the CF continued to increase slowly as if gas was slowly flowing to that transducer.

Shots S7 and S65

In both of these experiments melamine was packed at 70% TMD without a disk over the ignitor end of the porous bed. In Shot S7, a previous compaction test discussed in Appendix B of Reference 2, the melamine was loaded into a PMMA tube and the only instrumentation was a framing camera. The same type of ignitor as in Shot S65, although from a different batch, compacted the melamine with a slower particle velocity to a final compaction of 75.3% TMD versus 80.5% TMD in Shot S65. Presumably, the differences between Shots S7 and S65 were not caused by the different materials used for the plastic tubes, but rather were caused by different ignitor burning rates. This indicates the need in quantitative comparisons of data from compaction and DDT testing for a transducer to monitor the pressure of the ignitor gases.

The loaded Lexan tube in Shot S65 was observed with flash radiography and high-speed photography. The radiographic data in Figure 13a show dynamic data at only 505 μs since the CF had already reflected before the second radiograph at about 750 μs. Although straight line segments are drawn on the dynamic data, a continuous increase in compaction from just slightly more than 70% TMD at the CF to about 80% TMD at the driven end of the bed may be more representative.

The trace in Figure 13a for the final position of the x-ray tracers, as well as the corresponding traces for the preceeding melamine experiments, does not extrapolate to $\Delta x = 0$ at the far boundary as did the corresponding traces for the Teflon 7C experiments. Like the Teflon 7C experiments, the melamine probably

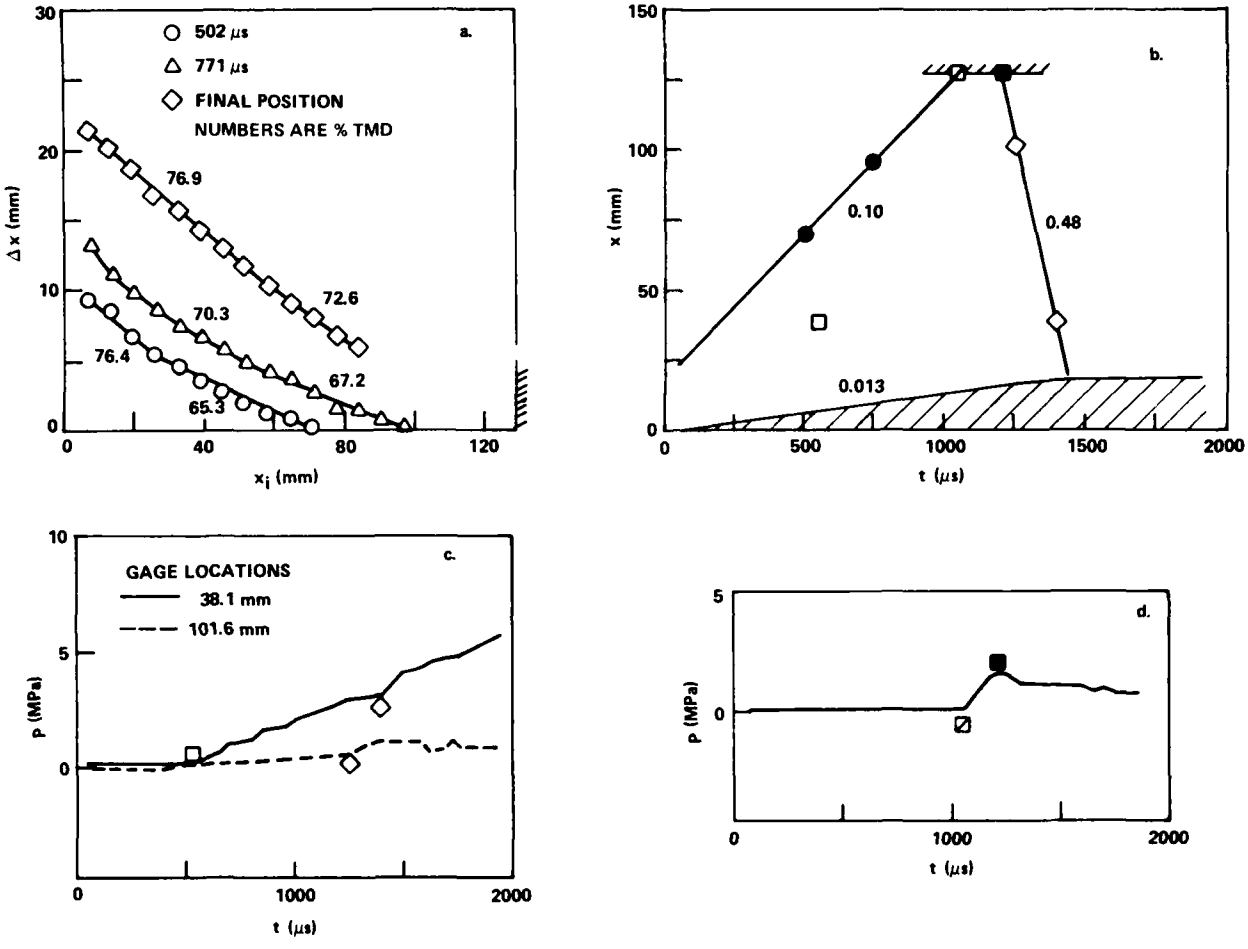

FIGURE 12. DATA FOR IGNITOR COMPACTION OF 60% TMD MELAMINE, SHOT S69
(REFER TO FIGURE 3 FOR THE KEY)
a. AXIAL DISPLACEMENT OF POROUS BED FROM RADIOGRAPHS
b. DISTANCE-TIME PLOT
c. STRAIN GAGE TRACES
d. FAR BOUNDARY (127.0 mm) PRESSURE TRANSDUCER TRACE

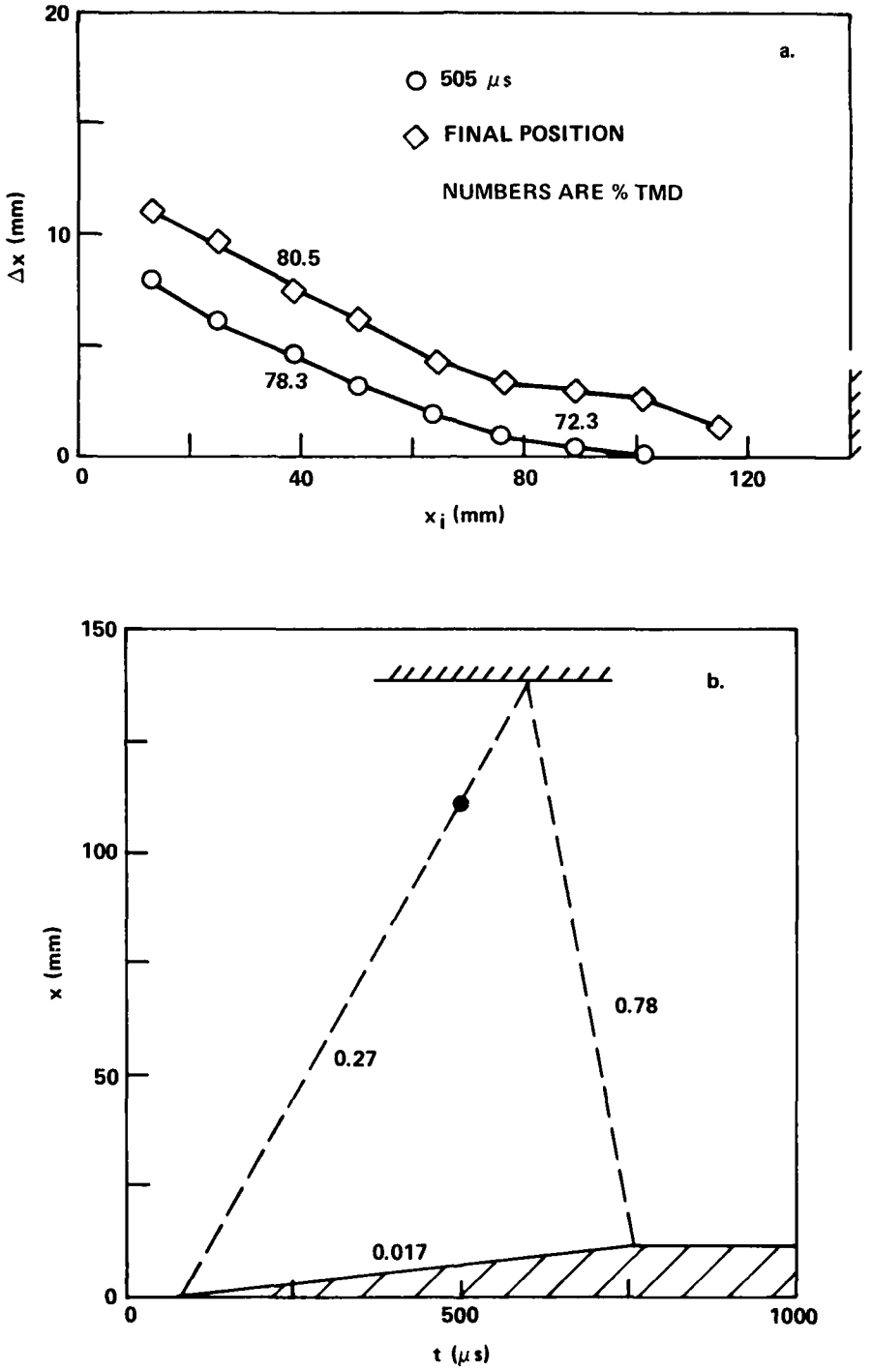

FIGURE 13. DATA FOR IGNITOR COMPACTION OF 70% TMD MELAMINE, SHOT S65 (REFER TO FIGURE 3 FOR THE KEY)
a. AXIAL DISPLACEMENT OF POROUS BED FROM RADIOGRAPHS
b. DISTANCE-TIME PLOT

was compacted uniformly following the propagation of the reflected CF; however, compacted melamine has little mechanical strength so when expansion waves unloaded the bed it tended to separate at several locations mostly at the far end of the bed. These separations are clearly visible on the radiographs.

The CF velocity was graphically estimated in Figure 13b as 0.27 mm/μs from the location of the CF at 505 μs and the onset of bed movement. As seen in Table 2, CF velocity increases as the initial density increases and the bed becomes less compressible.

In view of the density gradient in the compacted zone like in Shots S77 and S69, it is expected that the particle velocity at the CF will also be less than that at the driven end of the porous bed. So the particle velocity for both Shots S65 and S70, the next experiment to be discussed, is listed in Table 2 as less than the expansion rate of the luminous ignitor products.

Shot S70

The action of an ignitor on 80% TMD melamine resulted in such rapid propagation of the CF that it reflected at the far boundary before even the first radiograph at 503 μs; therefore, the radiographic data in Figure 14a have only the final position of the x-ray tracers. As shown in Figure 14b, the zone of luminous ignitor products stopped expanding at about 250 μs indicating the arrival of the reflected CF at the driven end of the bed. This time was much shorter than in other experiments; and the SG traces in Figure 14c show pressures and rates of pressurization much higher than in other experiments. Assuming that the onset of rapid pressurization at the 101.6 mm SG location corresponds to the arrival of the CF, a 0.42 mm/μs CF velocity was graphically estimated in Figure 14b. In only this experiment, a weak luminous front ahead of the end of the bed, which indicates gas flow along the inner tube wall, was filmed probably because of the high pressures at the ignitor.

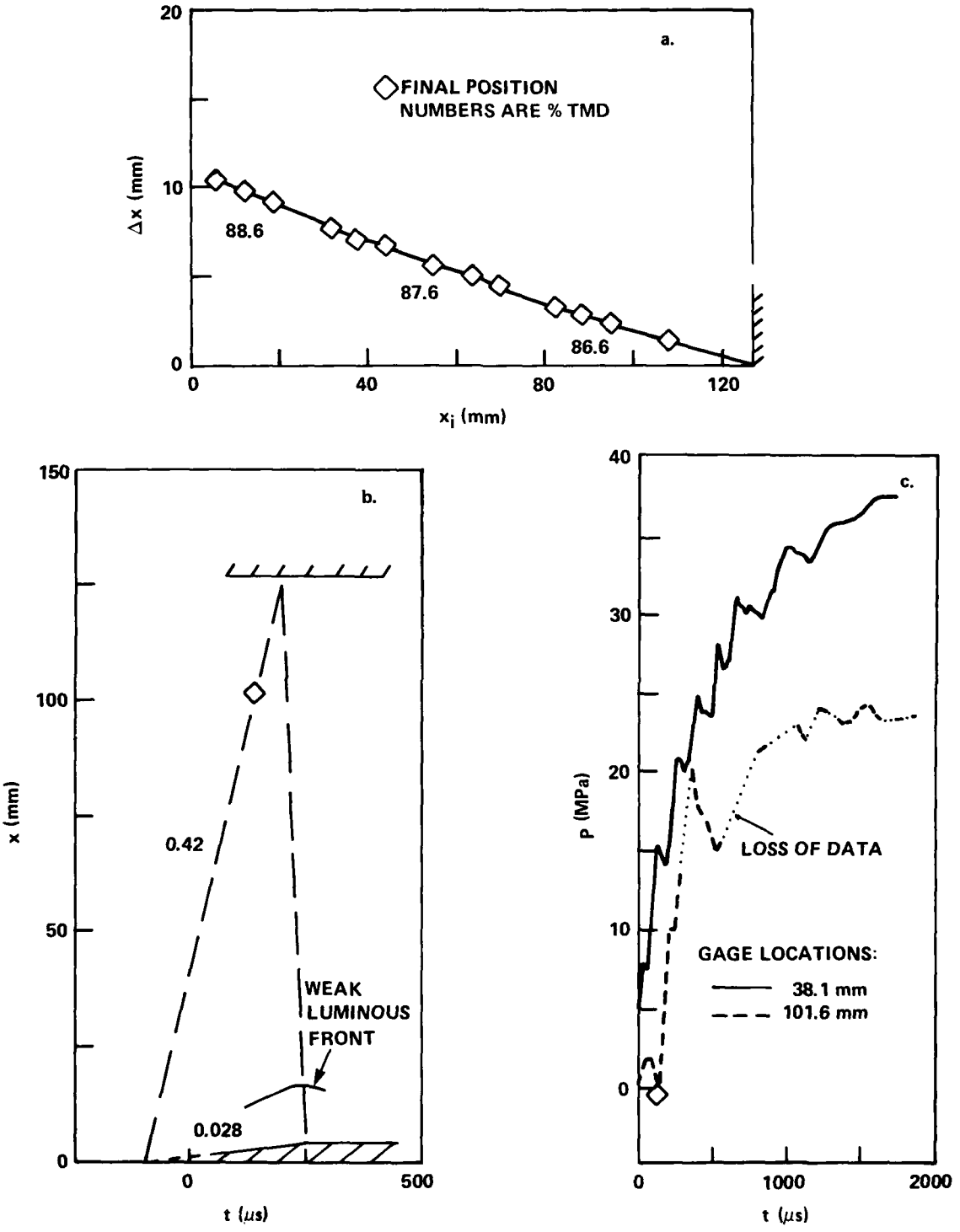

FIGURE 14. DATA FOR IGNITOR COMPACTION OF 80% TMD MELAMINE, SHOT S70
(REFER TO FIGURE 3 FOR THE KEY)
a. AXIAL DISPLACEMENT OF POROUS BED FROM RADIOGRAPH
b. DISTANCE-TIME PLOT
c. STRAIN GAGE TRACES

CHAPTER 4

DISCUSSION

ROLE OF IGNITOR DRIVEN COMPACTION IN DDT MECHANISMS

These compaction experiments demonstrated that the gaseous products of a standard NSWC DDT ignitor will drive a zone of increased density at least 130 mm into a porous bed. It was realized in earlier framing camera studies of DDT (see Section 4.B of Reference 2) that the ignitor products pushed the end of the porous bed from the ignitor and that the rate of displacement increased when the end of the porous bed ignited some 500 to 3500 μs after the first detection of luminous ignitor products. However, neither the extent of the increase in density nor the rate at which the compacted zone expanded was known. In view of results from the just completed study it is interesting to re-examine some of those experiments in Reference 2.

Picric acid (PA) was difficult to ignite relative to the other reactive materials; in Shot S41 ignition failed for a porous bed of 59.7% TMD PA. Using the Hugoniot relation for density, $\rho_h = \rho_o U/(U-u)$, with a 0.21 mm/μs CF velocity based on a piston gage response at the far boundary and a 0.041 mm/μs particle velocity based on the initial expansion rate of the luminous ignitor products, the compaction behind the ignitor driven CF was initially 74.2% TMD. This significant increase in density, along with melting of the PA, contributed to ignition failure by inhibiting convective heating of particles near the driven end of the bed. Also contributing to ignition failure was the compaction-generated reservoir between the porous bed and the ignitor which lowered the ignitor product pressure and, therefore, the heat flux to the PA. For two other tests with the same material, 68.2% TMD PA in Shot S51 ignited in 3.0 - 3.5 ms and 69.9% TMD PA in Shot S43 ignited in 1.4 - 1.6 ms; thus, increased ignitability correlates with decreased compressibility, that is, a smaller compaction-generated reservoir.

In Shots S43 and S51, the time to ignition was so long that the ignitor driven compaction front had time to propagate to the far end of the bed, reflect there, and then return to the driven end of the bed where it would reflect as an expansion wave. In Shot S43 the exact time of the reflection process at the driven end of the bed could not be determined from the camera film, but in Shot S51 with just a slightly lower initial compaction, 68.2% TMD, a clear camera film showed the end of the luminous ignitor product expansion at about 1.3 ms. This is near the time when ignition in Shot S43 was triggered possibly by the expansion wave breaking up the melt layer on the driven end of the bed.

A contributor to the difficult ignition of PA may be the release of ignitor product pressure from the end of the bed by a gap along the inner tube wall, this gap being caused by radial compaction. In Shot S83 (a 295.4 mm long column of

60% TMD Teflon 7C), it was postulated that the initial SG responses before the arrival of the CF resulted from gas flow in such a gap. Similar SG responses before the arrival of the CF occurred in the PA tests, but not in tests on fine and coarse tetryl, 97/3 RDX/wax and 96/4 RDX/wax, all of which more easily ignited than PA.[2]

One role of an ignitor driven CF is to desensitize a porous bed to compressive ignition by stronger compaction waves in the latter stages of the DDT mechanism, as was suggested in Reference 4 for a coarse HMX experiment. Ignitor driven compaction reduced the change in density and the associated particle shearing and deformation that occurred with the passage of the stronger CF through the bed. But when the stronger wave overtook the weaker one, the increased particle shearing and deformation was sufficient for compressive ignition.

This may explain the violent reaction at the far boundary that was reported in Reference 2 for a test with 46.2% TMD fine tetryl. There apparently was a 0.20 mm/μs ignitor driven CF with inner wall gas flow accompanying it according to SG responses and a weakly luminous 0.17 - 0.21 mm/μs front on the camera film (see Figure 7b. of Reference 2). Later a 0.32 mm/μs CF driven by tetryl combustion began propagating and should have overtaken the ignitor driven CF just before reaching the far boundary, possibly triggering the violent reaction there.

ANALYSES OF DYNAMIC AND QUASI-STATIC COMPACTION DATA

The ignitor product pressure driving the compaction process varied considerably as indicated, for example, by the 0.0mm transducer trace in Figure 5. Often this pressure was attenuated over the length of the compacted portion of the bed, especially for melamine as shown by the SG traces in Figure 11c, presumably because of wall friction. So a simple relation between driving pressure and compaction could not be obtained and, therefore, was not available for comparison with quasi-static data. As discussed in Reference 5, a successful comparison was obtained by using the quasi-static data as the compaction law in the computer simulation of two of the dynamic experiments, Shots S65 and S78; however, that model contained an approximate description of ignitor burning which possibly influenced the results.

Despite variations in the driving pressure, the compaction process at the front in the dynamic experiments was relatively steady for the ~130 mm long porous beds. This occurs because the inertia of the compacted zone will tend to continue the compaction. The CF velocity, in particular, appeared to remain constant during the dynamic experiments, even for the ~300 mm long bed in Shot S83.

In view of these observations, Hugoniot calculations for density, $\rho_h = \rho_0 U/(U - u)$, and pressure, $p_h = p_0 + \rho_0 U u$, were made using as input the dynamic measurements in Table 1 for U and u, and the quasi-static pressures in Figures 8 and 9 of Reference 5 for p_0 ($p_0 \equiv 0$ for Shots S77 & S69). These calculations are compared in Table 3 with experimental density (ρ_{cf}) and pressure (p_{cf}, based on 101.6 mm SG output) "just" behind the CF. The "just" distinction is required, especially for melamine, because of the variations in density and pressure along the compacted zone. Within experimental

error, jump condition calculations for both melamine and Teflon 7C agree with measurements. For Shots S65 and S70, the values for p_h are less than that listed because the values for particle velocity are less than that listed in Table 1.

Also shown in Table 3 are quasi-static pressures (p_q) from data in Figures 8 and 9 of Reference 5 corresponding to ρ_{cf}. Because quasi-static data for melamine did not extend below 70% TMD where it was rapidly changing, and because the dynamic radiographs in Shot S70 missed the propagation of the CF so that ρ_{cf} is unknown, p_q is listed for only one melamine experiment, Shot S65; however, for Shot S65 there is insufficient data for comparison with p_q. For Teflon 7C, the quasi-static pressures are only half of those required for dynamic compaction to the same density. Thus, compaction of Teflon 7C is rate sensitive.

Another approach for comparing quasi-static and dynamic compaction was to consider the p_q - %TMD plots in Figures 8 and 9 of Reference 5 as Hugoniot curves and then compute particle and CF velocities for changes in density corresponding to those in the dynamic experiments. When quasi-static compaction is adiabatic, which was essentially the case because not much heat was generated for dissipation at the less than 100 MPa pressures, the quasi-static relationship between pressure and density can be considered a Hugoniot curve. The Hugoniot relations define the CF velocity, U, and the particle velocity, u, in terms of the initial pressure and density, p_0 and ρ_0, and the final pressure and density, p and ρ, as

$$U = \frac{1}{\rho_0}\left(\frac{p - p_0}{1/\rho_0 - 1/\rho}\right)^{1/2}, \text{ and}$$

$$u = U\,(1 - \rho_0/\rho).$$

The Hugoniot calculations for melamine in Table 4 are in agreement with the measured velocities from the two dynamic tests with $(\%TMD)_0 \geq 70$, thus indicating that compaction of melamine is not noticeably rate sensitive. On the other hand, the calculations for Teflon 7C corresponding to Shot S83, for example, show calculated Hugoniot velocities significantly less than measured velocities, which again indicates the greater ease of quasi-statically compacting Teflon 7C. In view of the Teflon 7C results, the strain rate dependency of each material should be assessed.

The relationship between the compaction parameters is shown for Teflon 7C, for example, by the calculations in Table 4 based on quasi-static data in Figure 9 of Reference 5. For Teflon 7C initially at 60% TMD, increasing the final compaction from 70 to 85% TMD required a 388% increase in pressure which caused a 360% increase in particle velocity and a 177% increase in CF velocity. Particle velocity is nearly as sensitive as pressure to density changes, while CF velocity is only about half as sensitve. Thus, in Shot S83, the CF velocity could appear constant while the particle velocity decreased with the pressure.

TABLE 3. COMPARISON OF PRESSURES FROM DYNAMIC DATA AND HUGONIOT CALCULATIONS ON DYNAMIC DATA WITH QUASI-STATIC DATA

SHOT NO.	POROUS BED	$(\%\ TMD)_o$	$(\%\ TMD)^*_{cf}$	$(\%\ TMD)^{**}_h$	p_{cf}^* (MPa)	p_h^{**} (MPa)	p_q† (MPa)
S77	Melamine	60.0	69.0	66.7	1.2	1.1	---
S69	Melamine	60.0	66.2	66.7	0.4	0.9	---
S65	Melamine	70.0	72.3	74.7	----	<6.6	3.8
S70	Melamine	80.0	----	85.7	23.0	<28.5	---
S78	Teflon 7C	60.0	76.0	76.4	5.4	6.6	3.1
S79	Teflon 7C	60.0	81.9	80.7	8.5	9.9	5.3
S83	Teflon 7C	60.0	79.4	80.7	10.6	9.9	4.2

*$(\%TMD)_{cf}$, p_{cf} = Experimental density and pressure just behind the CF
**$(\%TMD)_h$, p_h = Hugoniot jump condition calculations for density and pressure behind the CF
†p_q = Quasi-static pressure[5] corresponding to $(\%TMD)_{cf}$

TABLE 4. HUGONIOT CALCULATIONS ON QUASI-STATIC DATA

POROUS BED MATERIAL	INITIAL STATE		FINAL STATE		HUGONIOT CALCULATIONS		COMPARATIVE DYNAMIC TEST
	$(\% \text{ TMD})_o$	P_o (MPa)	% TMD	P (MPa)	u (mm/μs)	U (mm/μs)	
Melamine	70	1.5	75	6.0	0.016	0.247	S65
Melamine	80	13.7	85	31.3	0.029	0.487	S70
Teflon 7C	60	0.8	70	1.8	0.010	0.070	
Teflon 7C	60	0.8	75	2.8	0.017	0.085	
Teflon 7C	60	0.8	80	4.5	0.026	0.103	S83
Teflon 7C	60	0.8	85	7.0	0.036	0.124	

CHAPTER 5

SUMMARY AND CONCLUSIONS

In order to improve our understanding of the role of the ignitor in the DDT mechanism, we have extended experimentally the gas driven compaction of inert porous beds, using the ignitor specified for NSWC DDT testing. Two inert materials, Teflon 7C and melamine, were chosen to represent the variation in mechanical properties for energetic materials used in DDT testing while avoiding the complications of violent reaction. These experiments were part of a research effort[5] that included quasi-static measurements of intragranular stress versus porous bed density and the implementation of those measurements into a numerical model which successfully simulated two of the dynamic compaction experiments.

The experimental arrangement, which was basically that used for transparent tube DDT testing, was well instrumented including a high-speed framing camera, two flash radiography channels, strain gages on the exterior of the confining tube, and one or more pressure transducers in direct contact with the porous bed. In this arrangement, a compaction front would propagate the 127 - 295 mm to the rigid boundary at the far end of the porous bed, reflect there as a stronger wave that further compacted the porous bed as it arrested the bed motion, and then reflect at the driven end of the bed as an expansion wave that reduced the bed pressure to the ignitor product pressure. In a DDT experiment usually only the ignitor driven compaction wave is of interest since a faster event most likely overtakes it before reaching the far boundary.

In high porosity beds packed at 60% TMD, an ignitor driven compaction front propagated at 0.14 mm/μs in Teflon 7C and 0.10 mm/μs in melamine. Just behind the compaction front, the 60% TMD bed of Teflon 7C was compacted to 76% TMD whereas melamine was compacted to only 66% TMD. The difficulty of compacting melamine relative to Teflon 7C is in agreement with quasi-static data.[5] A comparison for Teflon 7C of dynamic pressure versus density with quasi-static data indicated that dynamic compaction required about twice the quasi-static pressure to achieve the same density. Such a comparison for melamine was not possible because of the significant density gradient in dynamic experiments that was attributed to wall friction, which according to quasi-static data in a polished steel tube,[5] is an order of magnitude greater than for Teflon 7C. However, treating melamine quasi-static data as a Hugoniot curve and then calculating parameters for comparison with dynamic measurements indicated that melamine compaction may not be rate sensitive, at least not to the extent that Teflon 7C is. This type of analysis of quasi-static data also verified the experimental observations that 1) compaction front and particle velocity markedly increase with increasing initial density and 2) the particle velocity is more sensitive than the compaction front velocity to changes in compaction pressure.

Gas flow into the porous beds was not significant for both Teflon 7C and melamine because the bed particles were small (<60 μm). Inhibiting gas flow into the beds with a free-sliding disk on the ignitor end of the bed resulted in slight increase in compaction, compaction front velocity, and particle velocity, possibly because the disk promoted gas flow along the inner tube wall. The solid ignitor products on the inner tube wall after each Lexan tube experiment, and in one steel tube experiment, indicated localized gas flow there. In some experiments, especially those with a disk or with high initial density, gas flow along the inner tube wall was concurrent with the compaction front propagation but not necessarily extending to the front. An experiment designed to explore this phenomenon showed that the gas flow occurred in an annulus created by radial compaction of the porous bed rather than by tube expansion. Obviously, tube expansion will become significant as gas pressure increases. The effects of the annulus are: 1) to eliminate bed friction with the inner tube wall and thereby, aid compaction and 2) to extend burning along the lateral surface of a porous bed in a DDT experiment. Because strain gages are inexpensive and can be easily mounted on the outer wall of the confining tube, considerable effort was made to correlate the strain gage output (and piezoelectric transducer output) with gas flow along this annulus and propagation of the CF.

This study has aided the identification of ignitor driven compaction in DDT experiments, including the rate at which the fronts propagate, how far they can propagate, and by what extent the bed is compacted. Also, this study has suggested and confirmed several effects of ignitor driven compaction in the DDT mechanism. The initial formation of a cavity next to the ignitor reduces the pressurization and heat transfer process at the end of the porous bed; this delays the ignition of the bed material and the onset of conductive burning. The next stage of reaction, convective ignition, is propagated by convection of hot gases through the bed. It is inhibited by both the reduced pressure from formation of a cavity and the reduced permeability from ignitor driven compaction. The final stage of burning, compressive ignition, results from the rapid collapse of the porous bed by a strong compressive wave driven by bed combustion. Since the downstream region of the porous bed not yet compacted by the ignitor driven front is more sensitive to compressive ignition, the overtaking of the ignitor driven front by a strong compressive wave has been observed to coincide with the onset of compressive ignition.[4]

More experimentation is required to outline the compaction process for energetic materials during all stages of the DDT mechanism. The goals of future work will be to obtain dynamic data, to assess the adequacy of quasi-static data for a compaction law in computer modeling, and to understand more thoroughly the role of compaction in the DDT mechanism, especially the final stages.

REFERENCES

1. Bernecker, R. R., Sandusky, H. W., and Clairmont, A. R., Jr., "Compaction and the Burning to Detonation Transition at Low Confinement," Proceedings of 16th JANNAF Combustion Meeting, CPIA Publ. 308, Vol. 1, 1979, pp. 91-116.

2. Sandusky, H. W., and Bernecker, R. R., Transparent Tube Studies of Burning to Detonation Transition in Granular Explosives, Preliminary Framing Camera Studies, NSWC TR 79-79, 27 Oct 1980.

3. Butcher, A. G., Keefe, R. L., Robinson, N. J., and Beckstead, M. W., "Effects of Igniter and Compaction on DDT Run Up in Plastic Pipes," Seventh Symposium (International) on Detonation, NSWC MP 82-334, Naval Surface Weapons Center, 1982, pp. 143-150.

4. Bernecker, R. R., Sandusky, H. W., Clairmont, A. R., Jr., "Deflagration-to-Detonation Transition Studies of Porous Explosive Charges in Plastic Tubes," Seventh Symposium (International) on Detonation, NSWC MP 82-334, Naval Surface Weapons Center, 1982, pp. 119-138.

5. Sandusky, H. W., Elban, W. L., Kim, K., Bernecker, R. R., Gross, S. B., Clairmont, A. R., Jr., "Compaction of Porous Beds of Inert Materials," Seventh Symposium (International) on Detonation, NSWC MP 82-334, Naval Surface Weapons Center, 1982, pp. 843-856.

6. Bernecker, R. R., and Price, D., Sensitivity of Explosives to Transition from Deflagration to Detonation, NOLTR 74-186, 7 Feb 1975.

7. Elban, W. L., Gross, S. B., Kim, K., Bernecker, R. R., Quasi-Static Compaction of Porous Columns of Inert Materials in Support of DDT Studies, NSWC TR 81-113, to be published.

8. Baumeister, T., ed., Standard Handbook for Mechanical Engineers (New York: McGraw Hill Book Company, 7th Edition), p. 3-35.

NOMENCLATURE

Abbreviations:

CF	Compaction front
DDT	Deflagration-to-detonation transition
PA	Picric acid
PMMA	Polymethylmethacrylate
SG	Strain gage

Physical parameters:

L	Initial bed length
p	Pressure
t	Time
TMD	Theoretical maximum density
u	Particle velocity
U	Wave (CF) velocity
x	Axial distance
Δx	Axial displacement
ρ	Density

Subscripts:

c	Compacted
cf	Just behind the CF
f	Final
h	Hugoniot jump condition calculations
i	Initial position
o	Initial state
q	Quasi-static

APPENDIX A

RESPONSE OF STRAIN GAGES ON A LEXAN TUBE TO INTERIOR PRESSURE

The study of DDT in porous beds, as well as the related problem of dynamic compaction considered here, is aided by the measurement of pressure at various locations in the porous bed (see Reference A-1, for example). The often preferred measurement of axial pressure is difficult because the probe must be able to move with the porous bed. Consequently, measurements are often made at the inner tube wall so the probe can be securely mounted. In the case of piezoelectric materials packaged in a transducer body, a good assessment of pressure on the inner tube wall can be made as long as the interaction between the tube and the transducer body at high strain rates and pressures does not affect the output or at least can be accounted for. These transducers and the machining for mounting them are costly, especially in DDT testing where the tranducers as well as the tube would be destroyed. A cheaper, but less quantitative, continuous recording pressure probe which has been used is the externally mounted strain gage (SG). However, the qualitative and quantitative interpretation of responses from SG's mounted on Lexan tubes in DDT experiments[A-2] was difficult and has been no easier for these compaction studies.

The objective of this appendix is to show the response of SG's to various conditions on the inner tube wall. The first conditions discussed are static and dynamic gas pressurization at the SG location when the tube is empty and when the tube has a close fitting rod inside it at the SG location. The other condition discussed is solid stress on the inner tube wall from a porous bed that is being dynamically compacted by a piston.

A description of the SG's and their Wheatstone bridge circuitry, and the equations relating Wheatstone bridge output to circumferential strain on the exterior tube wall and that strain to inner tube wall pressure are in Appendix A of Reference A-3. The material constants used for the Lexan tube in the equations are: Young's modulus=2378 MPa (345,000 psi) and yield stress in tension = 58.6 MPa (8500 psi).

STRAIN GAGE RESPONSES TO STATIC AND DYNAMIC GAS PRESSURES IN A LEXAN TUBE

Static gas pressurization of the Lexan tube tested the integrity and response of SG's at two locations, 34.9 and 104.8 mm from the inlet end of the tube. In the static tests the junction plate and gas reservoir referred to in Figure A-1 were replaced by a plate with a central orifice connected to a solenoid valve, which was in turn directly connected to the gas supply. The first test had the solid rod in place as shown in Figure A-1 except the O-ring seal on the closure plate stem was moved to 9.5 mm from the left end of the solid

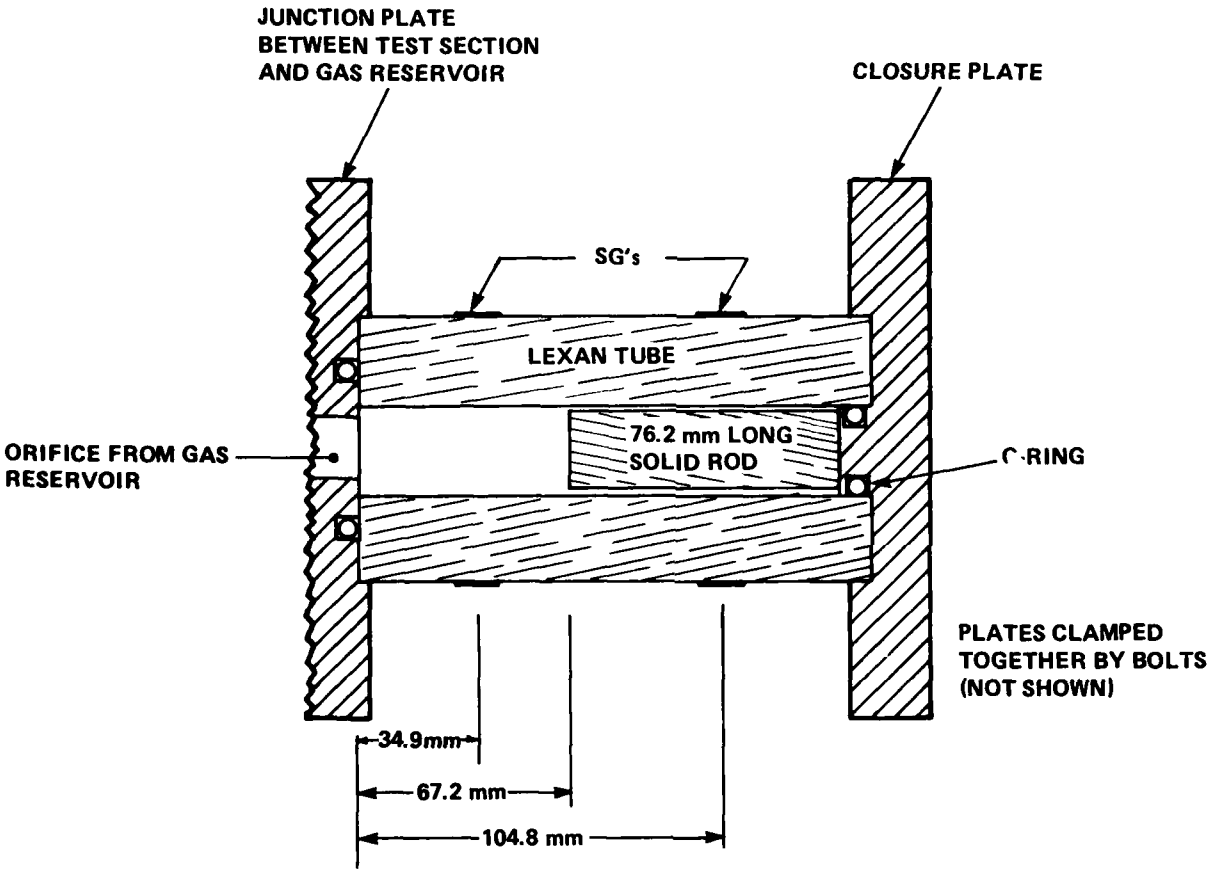

FIGURE A-1. TEST SECTION ARRANGEMENT FOR SG RESPONSES TO GAS PRESSURIZATION OF A LEXAN TUBE

rod. In this configuration, no gas pressure was on the inner tube wall at the 104.8 mm SG location. This was intended to indicate to what extent during a dynamic compaction or DDT experiment that a SG might respond before the tube as its location was pressurized.

The closed symbols in Figure A-2 are calculated pressures from the SG responses over an actual pressure range of 0 - 26.5 MPa (3850 psi); the dashed line is a reference showing calculated pressures equal to actual pressures. The 104.8 mm SG response showed that the pressurized section of the tube caused some tube expansion in the section where there was no gas pressure. Obviously, this spurious pressure would increase the closer that SG was to the pressurized section of the tube. Although this was a static test, tube expansion beyond the pressurized region should propagate at the shear velocity in the Lexan tube (0.908 mm/μs at 25°C),[A-4] which is faster than observed waves in the porous beds investigated in this study.

The plastic tube on which SG's are mounted is a poor heat sink for the increased heat that is generated as the gages are strained, and these isoelastic alloy gages generate significant thermally-induced apparent strain. So a second static test was performed in a short time period (< 1 second) to eliminate temperature effects which had to be calculated out of results from the first static test. For this second or quasi-static test, the solid rod shown in the tube in Figure A-1 was removed and the closure plate was replaced with one that had a piezoelectric transducer mounted in it to determine actual pressure. The gas lines leading to the apparatus were pressurized, and then the solenoid valve was opened allowing the test section to pressurize at a maximum rate of 0.22 MPa/ms. The open symbols in Figure A-2 are calculated pressures from the SG responses over an actual pressure range of 0 - 4000 psi (27.6 MPa). The quasi-static responses at both gage locations closely agree with each other and with the static response at the 34.9 mm gage location. Below 15 MPa the SG's respond as predicted, whereas beyond 15 MPa the SG's indicate higher than actual pressure as if Young's modulus decreased to 295,000 psi (2030 MPa). This is not surprising since Lexan is a viscoelastic material.

For the dynamic SG tests the arrangement shown in Figure A-1 was used. The gas resevoir had a brass diaphragm separating the 2000 psi (13.8 MPa) nitrogen in the reservoir from the test section until a pin ruptured the diaphragm. The pressures and rates of pressurization were similar to those experienced by burning an ignitor in the Teflon 7C compaction experiments. This apparatus was designed to study room temperature gas compaction of energetic materials; it will be described in more detail in future reports.

A typical response from the 34.9 mm SG is shown in Figure A-3a; the pressures were calculated using the same elastic constants as in the static test calculations. For comparison, the inner wall pressure measured by a piezoelectric transducer mounted at the same location in the wall of a steel tube is shown in Figure A-3b. The SG responded well to the rising pressure, but it was somewhat slower to respond than the transducer and does not record the peak pressure. The SG was less faithful after the peak was reached at about 800 μs; the tube appears to remain expanded indicating a 15 MPa pressure after the actual pressure declined to 11-12 MPa.

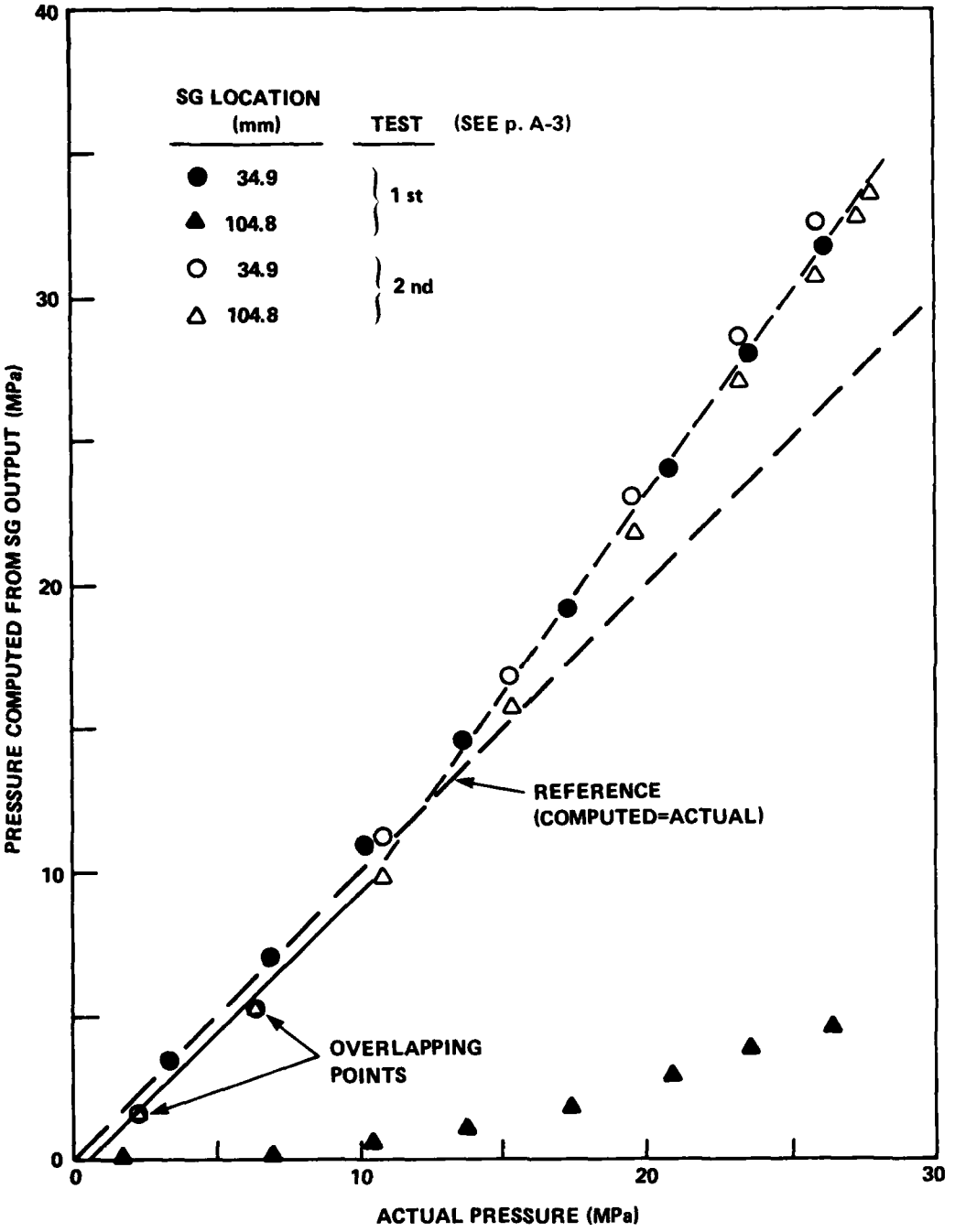

FIGURE A-2. STATIC CALIBRATIONS OF STRAIN GAGES ON A LEXAN TUBE

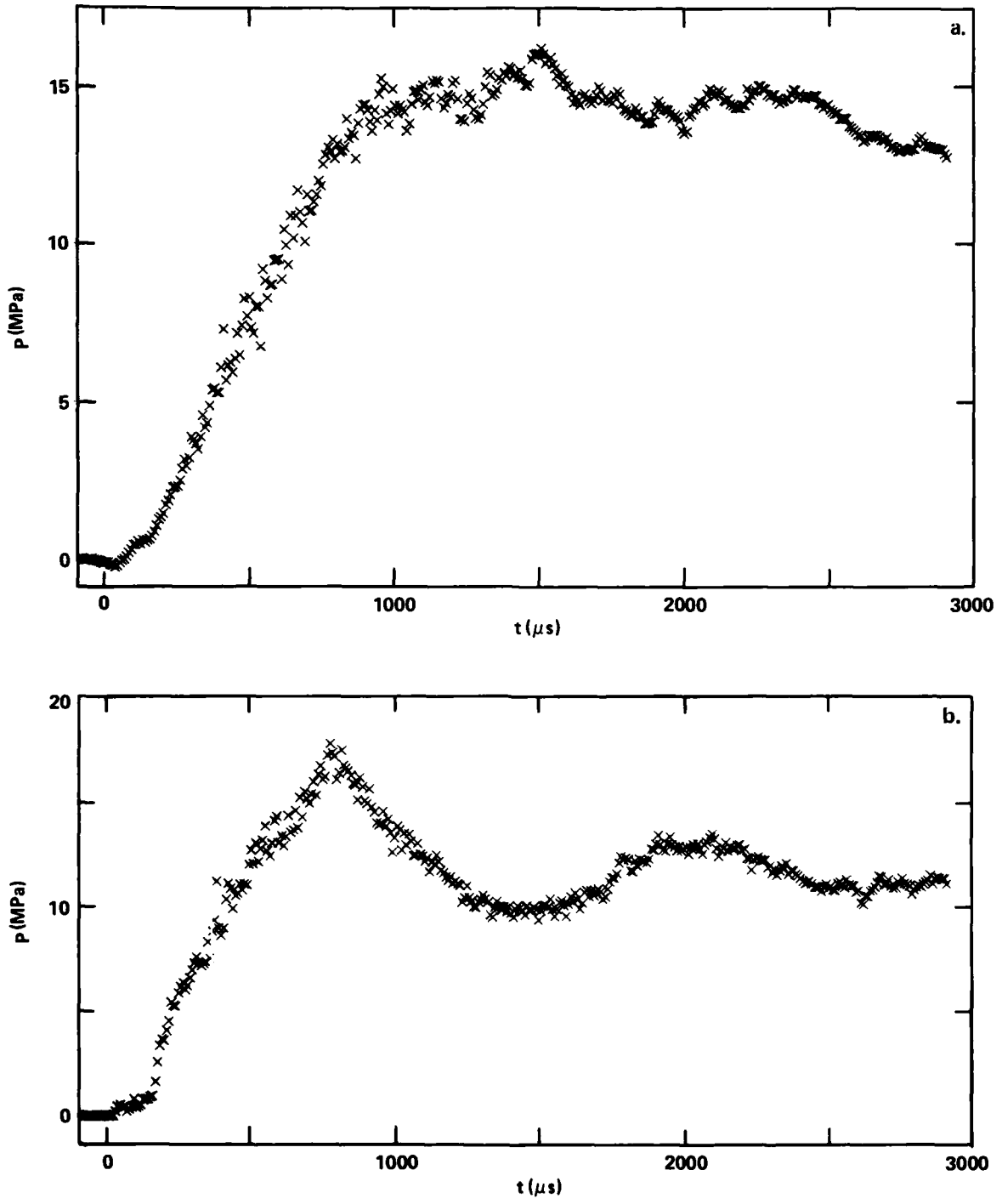

FIGURE A-3. COMPARISON OF STRAIN GAGE (a.) AND PRESSURE TRANSDUCER (b.) MEASUREMENTS AT x = 34.9 mm

Two different responses for the 104.8 mm SG are shown in Figure A-4. The response in Figure A-4a resulted when the solid rod in the tube shown in Figure A-1 was wrapped with adjacent, single thickness layers of tape and pressed into the Lexan tube. The SG response shows a declining, oscillating wave form added to a slowly rising pressure from gas leakage between the rod and the tube. The oscillating wave form probably represented two phenomena. The first small pressure rise is assumed to be from a shear wave originating from the pressurized section of the Lexan tube. The decline in pressure and the following oscillations are probably from the solid rod pushing against the closure plate.*

The SG response in Figure A-4b resulted when just the rod was in the tube, leaving an annulus of 0.16 mm (0.006"). The response was similar to that from the pressure transducer in Figure A-3b, except the SG response was delayed. As expected, the oscillations in Figure A-4a to some extent appear superimposed on the trace in Figure A-4b.

The traces shown in Figure A-4 aid the interpretation of SG records from the compaction experiments. Since elastic wave pressures would be relatively small for the porous beds that were investigated and since gas pressure in the zone between the ignitor and the end of the porous bed would only slightly expand the tube beyond that zone (see discussion of the first static test results shown in Figure A-2), significant SG response downstream of the compaction front (CF) must be from gas flow ahead of the CF. Furthermore, this gas flow occurs predominately along the inner tube wall (see discussion in Section 4). As shown in Figure A-4a, where there was initially a tight fit between the rod and the inner tube wall the small amount of tube expansion beyond the cavity allowed little gas flow along the inner tube wall. However, as shown in Figure A-4b, significant SG response occurred when only a small gap between the rod and the Lexan tube was available for gas flow. Strain gage responses in compaction experiments similar to those in Figures A-4b indicate the presence of a small gap at the inner tube wall and that this gap results predominately from radial compaction of the porous bed rather than tube expansion.

STRAIN GAGE RESPONSE TO A SOLID STRESS WAVE IN A POROUS BED CONFINED BY A LEXAN TUBE

Even in those compaction experiments in which a thin metal disk was over the ignitor end of the porous bed, some gas flow into the porous bed was present to influence the SG responses. It is desirable to know the contribution of solid

*Such an effect was observed when a solid rod was propelled through a Lexan tube and into the closure plate. The bolts clamping these apparatuses together axially stress the Lexan tube, which causes a circumferential strain that is equivalent to an interior pressure of above 6.5 MPa. Balancing of the strain gage circuitry eliminates this spurious pressure prior to a test. However, if the axial stress on the tube is released, for example, when a rod impacts the closure plate, the release of the preloaded strain in the tube now appears as the negative of the above spurious pressure. Then the elasticity of the bolts, which clamp the closure plate and tube together, quickly restress the tube more than it was at assembly resulting in a positive spurious pressure. The oscillations continue but attenuate.

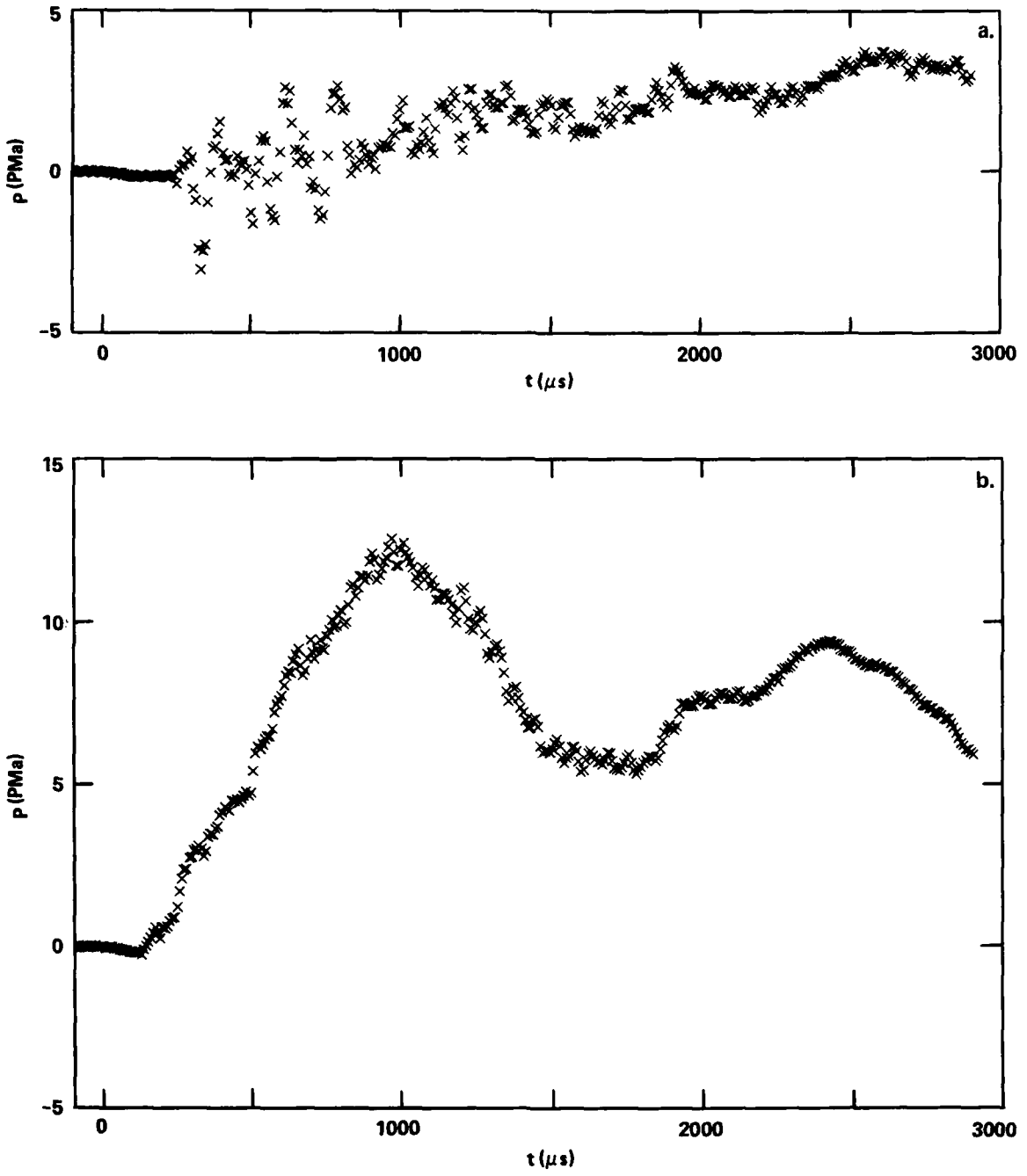

FIGURE A-4. COMPARISON OF STRAIN GAGE MEASUREMENTS AT x = 104.8 mm FOR A TIGHT (a.) AND LOOSE (b.) FITTING PLUG IN THE LEXAN TUBE

stress on the inner tube wall to SG response because this stress is the plastic yield pressure associated with porous bed compaction and because the relative contribution of gas pressure to the SG response can be ascertained. In order to remove the contribution of gas pressure from SG response, a test was conducted in which 60% TMD Teflon 7C was compacted by a flying piston.

The apparatus, which will be the subject of a future report, was developed for simulating dynamic compaction in energetic materials during the final stages of DDT. The piston (Lexan, 25.4 mm diameter by 305 mm long) was driven down a steel barrel by a combusting powder charge; the steel barrel is attached to a Lexan tube which confined the porous bed. For this test the mass of the typical powder charge was reduced in order to generate pressures in the porous bed comparable with pressures in ignitor driven compaction experiments. As shown in Figure A-5, there are slots at the barrel/Lexan tube interface for venting most of the air between the piston and the porous bed rather than forcing it into the porous bed. Instrumentation consisted of a SG on the Lexan tube at 63.5 mm from the driven end of the bed, a pressure transducer at the far end of the bed (146.1 mm), and four transparent disks in the porous bed which are backlighted by a xenon flash and filmed by a streak camera to record bed motion.

The strain gage trace in Figure A-6a shows first a decline in pressure, just as shown in Figures 4d and 3d, respectively for Shots S78 and S79, (also see comments on page 55 of Reference A-2), and then a rise in pressure associated with the CF. Interestingly, the initial rise in pressure occurs ahead of the CF by 120 μs, which, for example, is the same situation as in Shot S79. This initial pressure rise can be attributed to several effects. First, the static gas pressurization of a Lexan tube showed that inner wall pressure ahead of a SG location expanded the tube some at the SG location, thus causing a spurious pressure. Second, the edges of a SG are 4.8 mm on either side of the reported location of the center of a SG. Thus, some strain is seen before the stress wave reaches the center of the SG. Third, the pressure transducer trace in Figure A-6b. shows a weak precursor ahead of the CF. The first two of these effects was probably responsible for the observation that the SG trace is less steep than the pressure transducer trace, even though the compaction wave would be wider after propagating the distance from the SG to the pressure transducer. This same observation was noted in the dynamic gas pressurization of a Lexan tube; as shown in Figure A-3, the SG did not respond as fast as a pressure transducer at the same location.

When the SG first peaks at about 580 μs, the 16.8 MPa pressure compares well with a calculated jump condition pressure of 16.5 MPa based on the 0.058 mm/μs particle velocity of the disk preceding the SG location and the 0.195 mm/μs CF velocity. It was surprising that the SG recorded just after its first peak pressure a rapid decline in pressure to 13.8 MPa, which compares well with the 13.0 MPa jump condition pressure based on the 0.045 mm/μs particle velocity of the disk after the SG location. One explanation is that the piston partially unloaded the bed as evidenced by the larger decline in particle velocity between the second and third disks relative to that between the first and second disks. The piston length is such that it will maintain constant pressure on the end of the porous bed for about 270 μs, so a significant decline in pressure would be expected to reach the CF between the SG location and the third disk. However, the peak response of the SG occurred 150 μs after the CF passed the gage location; therefore, a lower pressure would be expected unless the tube did not relax as it did not in the test data shown in Figure A-3.

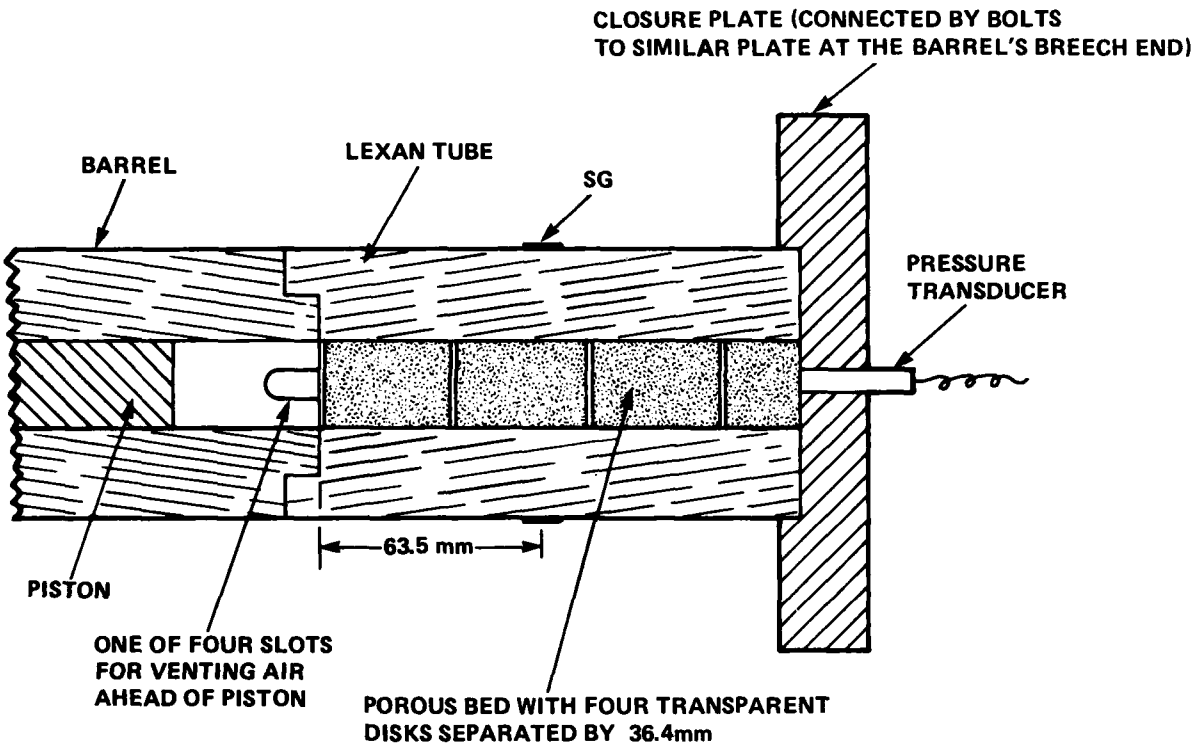

FIGURE A-5. TEST SECTION ARRANGEMENT FOR PISTON DRIVEN COMPACTION

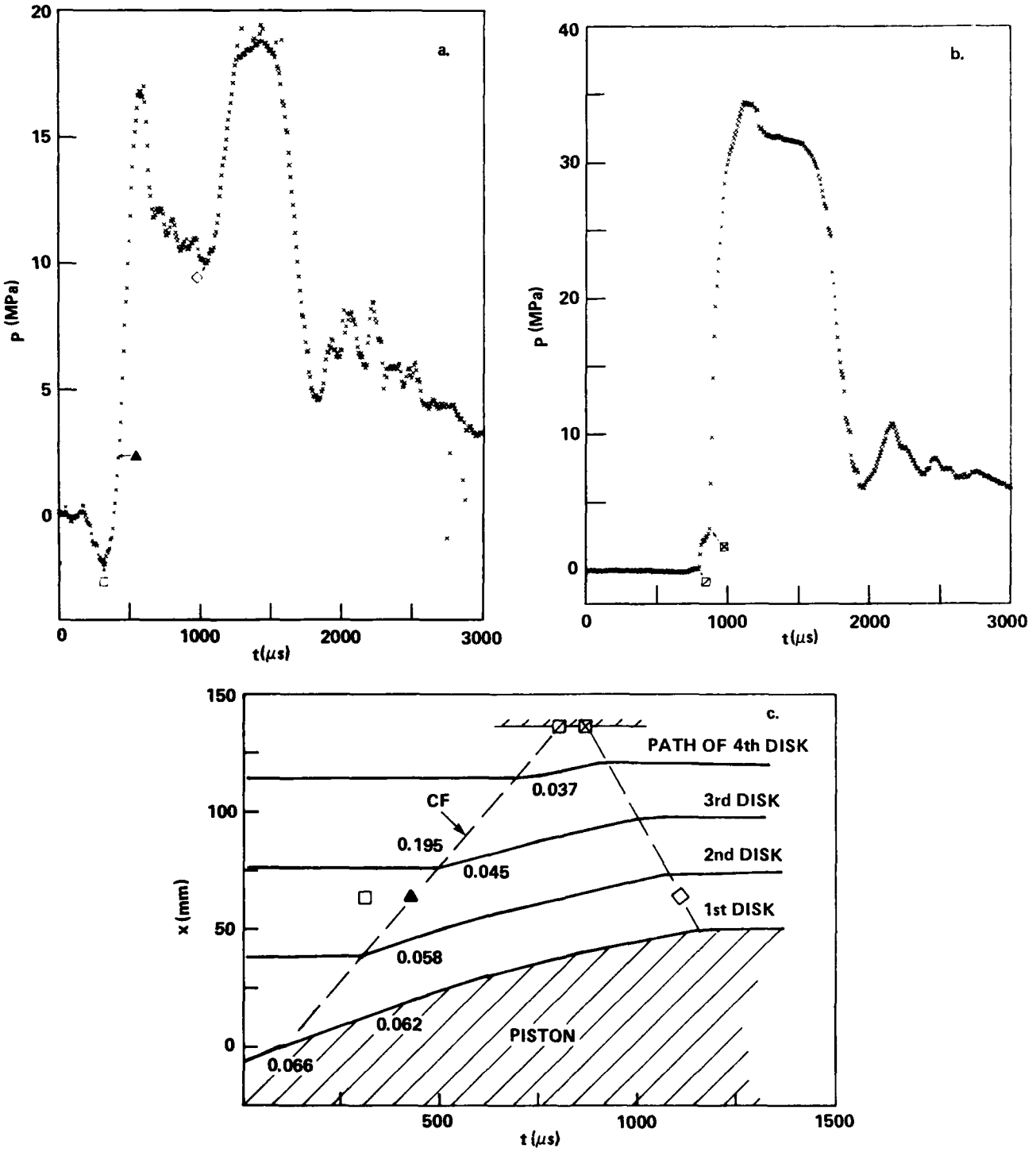

FIGURE A-6. DATA FOR PISTON DRIVEN COMPACTION OF 60% TMD TEFLON 7C (REFER TO FIGURE 3 FOR THE KEY)
a. STRAIN GAGE TRACE
b. FAR BOUNDARY TRANSDUCER TRACE
c. DISTANCE-TIME PLOT

When the CF encounters the rigid far boundary, the transducer trace in Figure A-6b first shows a weak precursor, possibly an elastic wave in the Teflon 7C, followed by a rapid rise in pressure. The refected CF which propagates back into the porous bed to arrest the particle velocity first reaches the SG location at 1112 μs. The peak pressure calculated from SG output for the rearward wave is only half of the pressure recorded by the transducer. Likewise, in the ignitor compaction experiments, SG's recorded pressures behind the rearward wave that were much lower in magnitude than pressures recorded by transducers at the far boundary. The peak transducer pressures agreed with jump condition calculations on rearward waves when adequate data existed for those calculations.

REFERENCES

A-1. Bernecker, R. R. and Price, D., "Studies in the Transition from Deflagration to Detonation in Granular Explosives. II. Transitional Characteristics and Mechanisms Observed in 91/9 RDX/wax.," Combustion and Flame, Vol. 22, 1974, p. 119.

A-2. Sandusky, H. W., and Bernecker, R. R., Transparent Tube Studies of Burning to Detonation Transition in Granular Explosives, Preliminary Framing Camera Studies, NSWC TR 79-79, 27 Oct 1980.

A-3. Bernecker, R. R. and Price, D., Transition from Deflagration to Detonation in Granular Explosives, NOLTR 72-202, 13 Dec 1972.

A-4. Asay, J. R. and Guenther, A. H., "Experimental Determination of Ultrasonic Wave Velocities in Plastics as Functions of Temperature, IV. Shear Velocities in Common Plastics," Journal of Applied Polymer Science, Vol. 11, 1967, pp. 1087-1100.

DISTRIBUTION

	Copies
Chief of Naval Material Department of the Navy Washington, D. C. 20360	1
Commander Naval Air Systems Command Attn: AIR-350	1
AIR-324A (B. Sopers)	1
Department of the Navy Washington, DC 20361	
Commander Naval Sea Systems Command Attn: SEA-99612	2
SEA-62R	1
SEA-62R2	1
SEA-62R3	1
SEA-62R32	1
SEA-64E	1
Department of the Navy Washington, DC 20362	
Director Strategic Systems Project Office (PM-1) Attn: SP2731 (J. Culver)	1
SP273 (E. L. Throckmorton)	1
Department of the Navy Washington, DC 20376	
Chief of Naval Research Attn: RADM L. S. Kollmorgen	1
ONR-432 (R. Miller)	1
ONR-741 (Technical Library)	1
Department of the Navy Arlington, VA 22217	
Commanding Officer Naval Propellant Plant Attn: Technical Library Indian Head, MD 20640	1
Office of Naval Technology Attn: MAT-07P (J. Enig)	1
MAT-0712 (E. Zimet)	1
Department of the Navy 800 North Quincy Street Arlington, VA 22217	
Commander Naval Weapons Center Attn: Technical Library	1
Code 3264	1
Code 3205 (C. Thelin)	1
Code 32050 (L. Smith)	1
Code 389 (R. Derr)	1
Code 3891 (T. Boggs)	1
Code 3891 (H. D. Mallory)	1
Code 3891 (K. Graham)	1
China Lake, CA 93555	
Director Naval Research Laboratory Attn: Technical Information Section	2
Washington, DC 20375	
Office of Naval Operations Operations Evaluation Group Group (OP03EG)	1
Washington, DC 20375	

DISTRIBUTION (CONT.)

	Copies
Director Defense Advanced Research Projects Agency Washington, DC 20301	1
Commanding Officer Naval Weapons Station Attn: R & D Division Code 50 Yorktown, VA 23691	1
Commanding Officer Naval Explosive Ordnance Disposal Facility Attn: Information Services Indian Head, MD 20640	1
Air Force Office of Scientific Research Attn: M. A. Stroscio L. H. Caveny Bolling Air Force Base Washington, DC 20332	1 1
Department of the Air Force AFRPL/DY, Stop 24 Attn: R. Geisler Edwards AFB, CA 93523	1
McDonnell Aircraft Company Attn: M. L. Schimmel P. O. Box 516 St. Louis, MO 63166	1
Commanding Officer Naval Ammunition Depot Crane, IN 47522	1
Commanding Officer Naval Weapons Evaluation Facility Attn: Code AT-7 Kirtland Air Force Base Albuquerque, NM 87117	1
Commanding Officer Naval Ammunition Depot Attn: QEL Concord, CA 94522	1
Superintendent Naval Academy Attn: Library Annapolis, MD 21402	1
Naval Plant Representative Office Strategic Systems Project Office Lockheed Missiles and Space Co. Attn: SPL-332 (R. H. Guay) P. O. Box 504 Sunnyvale, CA 94088	1
Hercules Incorporated Allegany Ballistics Laboratory Attn: Library P. O. Box 210 Cumberland, MD 21502	1
AMCRD 5001 Eisenhower Avenue Alexandria, VA 22302	1
Redstone Scientific Information Center U. S. Army Missile Command Attn: Chief, Documents Redstone Arsenal, AL 35809	2
Commanding Officer Army Armament Research and Development Command Energetic Materials Division Attn: Louis Avrami, DRDAR-LCE Dover, NJ 07801	1
Commanding Officer Harry Diamond Laboratories Attn: Library Keith Warner 2800 Powder Mill Road Adelphi, MD 20783	1 1

DISTRIBUTION (CONT.)

	Copies
Armament Development & Test Center DLOSL/Technical Library Eglin Air Force Base, FL 32542	1
Commanding Officer Naval Ordnance Station Louisville, KY 40124	1
Director Applied Physics Laboratory Attn: Library Johns Hopkins Road Laurel, MD 20707	1
U. S. Department of Energy Attn: DMA Washington, DC 20545	1
Research Director Pittsburgh Mining and Safety Research Center U. S. Bureau of Mines 4800 Forbes Avenue Pittsburgh, PA 15213	1
Director Defense Technical Information Center Cameron Station Alexandria, VA 22314	12
Goddard Space Flight Center, NASA Glenn Dale Road Greenbelt, MD 20771	1
Lawrence Livermore National Laboratory University of California Attn: M. Finger	1
E. James	1
E. Lee	1
P. Urtiew	1
C. Tarver	1
P. O. Box 808 Livermore, CA 94550	

	Copies
Sandia National Laboratories Attn: R. J. Lawrence, Div. 5166 P. O. Box 5800 Albuquerque, NM 87115	1
Director Los Alamos National Laboratory Attn: Library	1
R. L. Rabie	1
H. Flaugh	1
C. Forest	1
P. O. Box 1663 Los Alamos, NM 87544	
Chairman DOD Explosives Safety Board Attn: T. A. Zaker 2461 Eisenhower Avenue Alexandria, VA 22331	1
Aerojet Ordnance and Manufacturing Company 9236 East Hall Road Downey, CA 90241	1
Thiokol/Huntsville Division Attn: Technical Library Huntsville, AL 35807	1
Zernow Technical Service Center Attn: L. Zernow 425 W. Bonita Ave., Suite 208 San Dimas, CA 91773	2
SRI International Attn: D. Curran 333 Ravenswood Avenue Menlo Park, CA 94025	1
Thiokol/Elkton Division Attn: Technical Library P. O. Box 241 Elkton, MD 21921	1

DISTRIBUTION (CONT.)

	Copies
Teledyne McCormick Selph P. O. Box 6 Hollister, CA 95023	1
Lockheed Missiles and Space Co., Inc. P. O. Box 504 Sunnyvale, CA 94086	1
R. Stresau Laboratory, Inc. Star Route Spooner, WI 54801	1
Rohm and Haas Huntsville, Defense Contract Office Attn: H. M. Shuey 723-A Arcadia Circle Huntsville, AL 35801	1
U. S. Army Foreign Service and Technology Center 220 7th Street, N. E. Charlottesville, VA 22901	1
Princeton Combustion Research Laboratories, Inc. 1041 U. S. Highway One North Attn: M. Summerfield N. Messina Princeton, NJ 08540	1 1
Pennsylvania State University Dept. of Mechanical Engineering Attn: K. Kuo University Park, PA 16802	1
Director Ballistic Research Laboratories Attn: Library N. Gerri P. Howe R. Frey D. Kooker Aberdeen Proving Ground, MD 21005	1 1 1 1 1
Paul Gough Associates 1048 South Street Portsmouth, NH 03801	1
Hercules Incorporated, Bacchus Works Attn: B. Hopkins Library 100-H D. Caldwell P. O. Box 98 Magna, UT 84044	1 1 2
Professor H. Krier 144 MEB, University of IL, at U-C 1206 West Green Street Urbana, IL 61801	1
Chemical Propulsion Information Agency The Johns Hopkins University Applied Physics Laboratory Johns Hopkins Road Laurel, MD 20707	1
IIT Research Institute Attn: H. S. Napandensky 10 West 35th Street Chicago, IL 60616	1
Erion Associates, Inc. Attn: W. Petray 600 New Hampshire Avenue Suite 870 Washington, DC 20037	1
Brigham Young University Dept. of Chemical Engineering Attn: M. W. Beckstead Provo, UT 84601	1
Library of Congress Attn: Gift and Exchange Division Washington, DC 20540	4

DISTRIBUTION (CONT.)

	Copies
Commanding Officer Naval Underwater Systems Center Attn: LA 151 - Technical Library Newport, RI 02840	4
Superintendent Naval Postgraduate School Attn: Library Monterey, CA 93940	1
Internal Distribution:	
G21 (J. East)	1
E431	9
E432	3
R04	1
R10	1
R10B	1
R10C	1
R10D	1
R11	1
R11 (M. Kamlet)	1
R11 (T. Hall)	1
R11 (C. Gotzmer)	1
R11 (E. Anderson)	1
R12	1
R12 (J. Short)	1
R12 (L. Montesi)	1
R13	1
R13 (S. Jacobs)	1
R13 (D. Price)	2
R13 (R. Bernecker)	1
R13 (A. Clairmont)	1
R13 (H. Sandusky)	3
R13 (C. Coffey)	1
R13 (W. Elban)	1
R13 (K. Kim)	1
R13 (J. Forbes)	1
R13 (N. Coleburn)	1